EXPERIMENTAL INVESTIGATION INTO THE INFLUENCE OF TURBULENCE ON THE PERFORMANCE OF A SMALL-SCALE VERTICAL AXIS WIND TURBINE IN A WIND TUNNEL ENVIRONMENT

LODENYI KELVIN LWANGU

MASTER OF SCIENCE

(Physics)

JOMO KENYATTA UNIVERSITY OF

AGRICULTURE AND TECHNOLOGY.

2020

Experimental Investigation into the Influence of Turbulence on the Performance of a Small-scale Vertical Axis Wind Turbine in a Wind Tunnel Environment

Lodenyi Kelvin Lwangu

A thesis submitted in partial fulfilment for the Degree of Master of Science in Physics in the Jomo Kenyatta University of Agriculture and Technology.

2020

DECLARATION

This thesis is my original work and has not been submitted for a degree in any other university.

Signature……. Date……..

Lodenyi Kelvin Lwangu

This thesis has been submitted for examination with our approval as university supervisors

Signature……..... Date …….

Prof. J. N. Kamau, PhD

JKUAT, Kenya

Signature…….…… Date……

Dr. D. W. Wekesa, PhD

Multimedia University, Kenya

DEDICATION

I would like to dedicate my work to my father, John Lwangu; for earning an honest living and sacrificing so much for us and always encouraging me to be a better person; and my mother, Rose Ludia, most loving and most prayerful lady who always wanted me to cover this stage of life.

ACKNOWLEDGEMENT

Foremost, I would like to express my most humble and most sincere gratitude to God Almighty for good health, strength of will and every resource towards the success of this research.

Secondly, I dearly wish to appreciate my supervisors Prof. Kamau of Jomo Kenyatta University of Agriculture and Technology and Dr. Wekesa of Machakos University for their strict yet fatherly guidance and support of my research, their patience, enthusiasm, motivation and immense knowledge. I am grateful to the Physics Department fraternity, JKUAT for giving me this chance to study and for evaluating my work.

Thirdly, I wish to acknowledge the financial support extended to this research by the Government of Kenya National Research Fund (Grant No. NR-F/1/MMC/450) and the Mrs. Krishna Uppal Memorial Fund of the Jomo Kenyatta University of Agriculture and Technology. At my lowest moments they resurrected my energy. I am grateful to the staff at the JKUAT Mechanical Department Fluid Engineering Laboratory led by Mr. Waka for guiding me and being available when I needed them.

Finally, I wish to extend my gratitude to my dedicated father, mother and siblings for unwavering trust and encouragement. I appreciate my friends Dorothy Mwanzia, Evance Odero and Nicholas Mutiso who have been there with me throughout the study and ever willing to offer a hand when called upon. I am forever grateful for all your contribution to this research.

TABLE OF CONTENTS

LIST OF TABLES

LIST OF FIGURES

LIST OF APPENDICES

LIST OF SYMBOLS

ρ	Air density
U_{∞}	Free-stream wind speed
U_{mean}	Mean speed of unsteady wind
$\bar{u}$	Overall mean wind speed
$u(t)$	Fluctuating wind as a function of time
u'_{sp}	Short period fluctuations in the order of seconds to minutes
u'_{lp}	Long period fluctuations in order of 10 to 100 hours
u_f	Frictional velocity
k	Von Karman's constant (0.40)
ω	Rotational speed
v	Tip speed ratio
f_c	Characteristic fluctuation frequency of the gust
D_g	Gust length
z	Height above the ground
z_o	Surface roughness

LIST OF ABBREVIATIONS AND ACRONYMS

ABL	Atmospheric boundary layer
AR	Aspect ratio
Ce	Energy coefficient
CFD	Computational fluid dynamics
C_m	Torque coefficient
CP	Power coefficient
3-D	Three dimensional
$E_{turbine}$	Extracted aerodynamic energy
E_{wind}	Total available wind
fps	Frames per second
GHG	Greenhouse gases
HAWT	Horizontal Axis Wind Turbine
N	Rotational speed per minute
NACA	National advisory committee for aeronautics
NI	National instruments
PBL	Planetary boundary layer
P_{blade}	Power produced by the turbine blades
P_{wind}	Power available in the wind
RANS	Reynolds Averaged Navier-Stokes
RPM	Revolutions per minute
RPM	Revolutions per minute
R_{rotor}	Rotor radius
T	Turbine blade torque
TI	Turbulence Intensity

TSR	Tip speed ratio
VAWT	Vertical Axis Wind Turbine
VFD	Variable frequency drive

ABSTRACT

Wind power is ranked among the fastest growing renewable energy technologies. Globally, there is renewed interest in research and utilization of wind energy both onshore and offshore. Horizontal axis wind turbines (HAWT) have been preferred because of existing knowledge on their performance and productivity. However, with an increasing global population and urbanization, there is higher demand of power in urban environments. The behavior of wind in these built-up areas is affected by extremely complex interaction amongst incident wind, vertical velocity gradient, shapes, sizes and layouts of buildings and resultant turbulence. In such conditions, small-scale wind turbines have been utilized as sources of power. Vertical axis wind turbines (VAWT) have proven particularly suitable for power production in these environments. The aerodynamic performance of VAWT operating in non-uniform turbulent flow regimes has not been comprehensively researched leaving a knowledge gap on their optimization and utilization for these environments. Different studies conducted on this field have not specifically agreed on the effect of turbulent non-uniform flow conditions on the performance of VAWTs. In this study an experimental method was used to investigate the effect of free-stream turbulence intensity on the aerodynamic performance of a VAWT under turbulent flow operating conditions in an open wind tunnel. To carry out the investigation, a mechanism to generate a turbulent flow was created to analyze the effect of induced turbulence intensity on the aerodynamic performance of a small-scale VAWT. The turbulence levels were chosen to match prevailing wind characteristics of the unsteady urban environment target site in Kenya. In addition, a systematic analysis of torque, power and energy coefficients, including their variations at uniform flow have been presented to predict the aerodynamic performance of a small-scale VAWT model. The VAWT was subjected to free-stream wind speeds ranging between 5 m/s and 10 m/s at different tip speed ratios. For uniform flow, the power coefficient, CP distribution power curve continued to increase with increasing free stream velocity throughout the range of TSR under study. The power increased up to an optimum CP of 0.2822 at uniform wind speeds of 10 m/s. Under the non-uniform conditions fluctuations in power production were recorded with the optimum power produced at CP of 0.36 at wind speed 5 m/s. The study findings revealed that non-uniform turbulent wind impacted the aerodynamic performance of the turbine with higher power coefficients being observed at lower wind speeds and improved self-starting ability in the presence of turbulence.

CHAPTER ONE

INTRODUCTION

1.1 Introduction

This chapter aims to introduce the work that was done in this thesis. The background of the study is outlined to bring out what advised the research work. The identified problem is stated with the justification for the study. Further, the objectives are outlined and the research scope explained.

1.2 Background of the study

For the longest time, the world has relied on burning of fossil fuels which is a non-renewable source of energy. These sources are dwindling and are expected to be depleted within the next century (John & Anthony, 2006). Equally, burning of fossil fuels results in the emission of Green House Gases that have largely contributed to global warming and the resultant climate change (Kaldellis & Zafirakis, 2011). This generation has seen some of the most dangerous and life threatening effects of climate change. It is important that as the world plans for its sustainable future, research and funding is directed towards finding sustainable alternative sources of energy (Moreno, Lopez & Garcia-Ivarez, 2012).

In response to the need for utilizing other sources of energy, recent focus has been directed to renewable energy sources. Fuel sources other than those derived from fossil fuels including wood and wood waste, landfill and biogas, ethanol, biodiesel, and municipal waste; geothermal power, hydropower, solar and wind energy provide the best alternative to the finite fossil fuels (Gagliano, Fransesco, Fransesco & Alfonso, 2013). These five sources are readily available, environment friendly, infinite and relatively cheaper if sufficiently researched (Manwell, McGowan & Rogers, 2009).

Wind energy source has increasingly been utilized since it is free, clean and readily available. Flowing wind has an associated kinetic energy (John & Anthony, 2006). Wind turbines will convert this kinetic energy into mechanical power through the rotation of turbines (Manwell *et al*., 2009). Traditionally, this mechanical power has been used in tasks like grain grinding or to pump water through the operations of a wind mill. The blades of the turbine capture the power in the wind by rotating and transmitting it down the shaft inside the nacelle (John & Anthony, 2006). The shaft spins a generator which converts this mechanical power by way of gears into electricity making it available for grid use and powering homes and businesses (Manwell *et al*., 2009; John & Anthony, 2006).

The harnessing of wind energy is done both at small scale and large scale. On large scale, a number of large wind turbines are used in a wind farm (Manwell *et al*., 2009). The power output of each turbine is connected with the rest and added to the grid. Small scale wind energy production utilizes small scale wind turbines that can be used for powering single homes and light industries (Gagliano *et al*., 2013, Wekesa, Wang, Wei & Zhu, 2016).

Urban environments constitute the largest consumers of electricity world over. In this environment, micro-generation of power represents an opportunity for development of renewable energy (Gagliano *et al*., 2013). Energy harvesting through wind turbines is an option that has been exploited and could yet be considered even further.

Wind energy is harnessed through wind turbines that convert kinetic energy in the wind to mechanical energy then to electrical energy. Turbines are divided into two depending on the orientation of their rotational axis to be either horizontal axis wind turbines (HAWT) or vertical axis wind turbines (VAWT). Due to their sensitivity to change in wind direction and turbulence phenomena, HAWT rotors have to be positioned in the direction of wind through a yaw motor or by means of a tail (Manwell *et al*., 2009). Effectively then, the best environments to position HAWT are open areas with smooth air flow and considerably few obstacles.

VAWTs on the other hand do not need to be positioned in the direction of wind since they are not significantly affected by the variation in wind (Mojtaba, Carriveau & Ting, 2015). This characteristic makes VAWTs suitable for urban environments. The effect of turbulence here may not significantly affect the power output. Impact of turbulence, however, is crucial especially for small wind turbines that are usually installed near the ground with obstacles such as buildings, trees, etc. which result in high levels of free stream turbulence (Mojtaba *et al*., 2015, Wekesa *et al*., 2016, Manwell *et al*., 2009).

1.3 Statement of the Problem

Characteristic fluctuating free stream associated with complex urban terrains present a significant challenge to the aerodynamic performance of vertical axis wind turbine operating in turbulent regimes (non-uniform winds). The concept of generating turbulent flow wind is not well established and is difficult to implement due to existing technical complexities under such conditions. In this study, an experimental method was used to investigate the effect of free-stream turbulence intensity on the aerodynamic performance of a VAWT. The flow physics causing this behavior under turbulent flow operating conditions in a wind tunnel was studied.

1.4 Justification of the Study

Urban environments are characterized by unsteady wind regimes. Small wind turbines, specifically VAWTs, offer a very good option for micro-generation of power in these environments. They can easily be integrated into the architectural designs of the cities by mounting on walls or positioned in spaces between the buildings that create a form of a wind tunnel.

In order to sustain this form of clean energy, a lot of scientific research should be conducted to advice on the potential, performance and viability of different turbines. While there is an increase of research on the aerodynamic performance of isolated turbines, most of the studies focus on steady conditions. The steady wind conditions are

by no means a representative of the actual unsteady wind performance in urban environments. Turbulent wind changes with time; and since wind power is proportional to the cube of wind speed, moderate fluctuations in wind speeds result in very large fluctuations in available power. This evidently exposes the existence of a knowledge gap on the behavior of wind turbines in unsteady environments. Very little research/literature exists on the systematic performance testing of VAWT under controlled turbulent flows with uniform and non-uniform wind conditions.

This study uses wedge generated turbulence as simulation for a built environment. Elliptical wedges were erected to span the wind tunnel length where the width represented the architecture of a built environment. The behavior of the design turbine used could be extrapolated to other design dimensions of the same VAWT. The results obtained from this research is fundamental in designing and optimization of wind turbines for maximum power production in urban and built environments. This form of power is environmentally friendly, cheap and readily available for use and can be harnessed well to reduce dependence on fossil fuels.

1.5 Hypothesis

Non-uniform turbulent conditions do not improve the performance of vertical axis wind turbines

1.6 Objectives

1.6.1 General Objective

To investigate effect of turbulence on the performance of a small-scale vertical axis wind turbine in a wind tunnel environment.

1.6.2 Specific Objectives

1. To design a wedge turbulence generating mechanism and create a turbulent wind in a wind tunnel
2. To measure the wind velocity and turbulence profiles in the wind tunnel
3. To measure and analyze wind power performance of VAWT in uniform and non-uniform turbulent conditions

1.7 Research scope

The scope of this study was to fabricate, assemble and test a vertical axis wind turbine rotor blade in a wind tunnel environment. The fabricated rotor adopted a NACA 0012 aerofoil profile. This was assembled into a three-bladed H-rotor capable of rotating under wind and producing measurable power. A turbulence generating mechanism was developed in the wind tunnel. The power performance of the rotor was measured and analysed under uniform and turbulent non-uniform conditions.

CHAPTER TWO

LITERATURE REVIEW

2.1 Introduction

This chapter presents the theoretical principles relevant to the understanding of wind power and its harvesting through wind turbines. Wind as a resource is described and the analytical formulations of fluctuating wind including assessment and gustiness are outlined. The chapter also looks at the interaction of airfoils with fluids in boundary layer. Mathematical expressions defining the characteristics of turbines and their interaction with fluids are also explained.

2.2 Theoretical principles of Wind energy

2.2.1 Wind

Wind is moving mass of air as a result of uneven heating of the atmosphere by the sun, variations in the earth's surface and the rotation of the earth. It can be classified as a by-product of solar energy with about 2% of the energy from the sun being converted to wind energy (Manwell *et al*., 2009). Wind flow patterns in different regions are influenced by infrastructure, water bodies, vegetation, mountains and other geographies. The heating of the sun varies due to these conditions where the air above the warmer areas heats up and reduces in density causing it to rise. The result is an area of low pressure that is then occupied by cooler air from areas of higher pressure. This characteristic movement of air between warmer regions and cooler regions result to a scenario called the wind.

2.2.2 Log-law and power law

Wind gradient is difference in wind speed and direction that usually occurs over small distances in the atmosphere. The two mathematical models commonly used to

approximate the wind velocity profile in the atmospheric boundary layer are log-law and power law. The logarithmic wind profile is expressed in equation 2.1 (Manwell *et al*., 2009, Wekesa, Wang, Wei & Danao, 2017):

$$\bar{u}(z) = \frac{\mu}{k} \ln\left[\frac{z}{Z_o}\right] \quad \text{.....2.1}$$

where: μ is the mean wind speed, z is the velocity above the ground, $\bar{u}$ is the shear velocity (m/s), k is the Von Karmans's constant (k = 0.40) and Z_o is the surface roughness length (m). The equation suggests that wind velocity increases logarithmically with increasing height within the boundary depending on the surface roughness and atmospheric stability. The stability term drops out for neutral stability conditions (adiabatic conditions). Therefore, power law is used to determine the velocity profile in cases of neutral stability. This study used the power law according to Manwell to describe the wind profile in the wind tunnel (Manwell *et al*., 2009, Wekesa *et al*., 2017) as equation 2.2:

$$\frac{u(z)}{u_{ref}} = \left[\frac{z}{z_{ref}}\right]^{\alpha} \quad \text{.....2.2}$$

where $u(z)$ is the wind speed at height z, u_{ref} is the reference wind speed at height Z_{ref} and α is the power law exponent that depends on the surface roughness and atmospheric stability.

2.2.3 Wind power

Power in wind depends on the speed of air (velocity) and mass of air (density) flowing through a flux or stream of air. Power is obtained from its kinetic energy given as equation 2.3.

$$K.E = \frac{1}{2} mv^2 \quad \text{2.3}$$

the mass of air can be determined from the density and air volume in equation 2.4:

$$m = \rho V \quad \text{2.4}$$

Inserting equation 2.4 into equation 2.3 yields equation 2.5:

$$K.E = \frac{1}{2} V\rho v^2 \quad \text{2.5}$$

Power is the rate of change of energy with time. When we consider a small time change ∂t and that air particles travel through a small distance $s = v\partial t$, we can obtain the volume by multiplying the distance with the rotor area in equation 2.6:

$$\partial V = Av\partial t \quad \text{2.6}$$

Power is then obtained by considering change of kinetic energy with time expressed in equation 2.7:

$$P_{wind} = \frac{\partial V \rho v^2}{2\partial t} = \frac{1}{2} \rho A v^3 \quad \text{2.7}$$

The power in the wind is directly proportional to the air density, cube of wind speed and rotor swept area.

2.2.4 Power performance parameters

The effective usable power is usually below the indicated power since all wind does not stop completely when it interacts with the turbine. The turbines allow air to pass through so that there is continuous movement and power extraction. Therefore, only a part of the kinetic energy can be extracted and this value was studied by a German Physicist, Albert Betz in 1919. The maximum value of obtainable power is 16/27 or

59.3% of the total power in wind. This is a theoretical value but in reality turbines do not achieve this value.

Power coefficient is the ratio of power extracted by the turbine to the power available in the wind denoted as CP. CP gives the ratio of the actual electric power produced by the wind turbine divided by the total wind power flowing into the turbine blades at a specific wind speed. The Power coefficient, CP varies with operating conditions such as wind speed, rotation speed and blade angle among other factors. It is used as a measure of the turbine's overall system efficiency. Having the CP at a given wind speed will help estimate the electric power output (Manwell *et al*., 2009, Wekesa, Wang, Wei, Kamau & Danao, 2015). Including CP, equation 2.7 becomes equation 2.8:

$$P_{turbune} = \frac{1}{2}\rho A v^3 Cp \quad \text{..... 2.8}$$

Power coefficient and torque coefficient are dimensionless performance parameters that are commonly used to characterize aerodynamic performance of wind turbines. They are defined as functions of tip speed ratio λ (Manwell *et al*., 2009) as torque coefficient equation 2.9:

$$C_m = \frac{T}{\left(\frac{1}{2}\rho A R U_\infty^2\right)} \quad \text{..... 2.9}$$

power coefficient is calculated as in equation 2.10:

$$CP = \frac{P_{Blade}}{P_{Wind}} = \frac{T_\omega}{\frac{1}{2}\rho A U_\infty^3} = \frac{T}{\frac{1}{2}\rho A U_\infty^2 R_{Rotor}} \frac{\omega R_{Rotor}}{U_\infty} = C_m \times \lambda \quad \text{.....2.10}$$

while the tip speed ratio is given as equation 2.11:

$$\lambda = \frac{\omega R_{Rotor}}{U_\infty} = \frac{2\pi N}{60} \frac{R_{Rotor}}{U_\infty} \quad \text{.....2.11}$$

where; T is the turbine blade torque, ρ is the air density, U_{∞} is the free-stream wind speed, R_{Rotor} is the rotor radius, P_{Blade} is the power produced by the turbine blades, P_{Wind} is the power available in the wind, ω is the rotational speed, and N is the rotational speed per minute (rpm). This study uses these parameters in the data analysis to characterize the power performance for the rotor in both uniform and non-uniform conditions.

2.2.5 Atmospheric Boundary Layer

This is the lowest part of the atmosphere also called the planetary boundary layer (PBL). It has a depth in the order of 1000 meters. It can be divided into an upper layer that comprises about 90% and an inner or surface layer that is about 10%. Direct influence of the surface characteristics are observed in the surface layer. The flow field in this layer is influenced by the interaction with the earth surface. In this section, physical properties such as flow velocity, temperature and moisture display rapid fluctuations and experience strong vertical mixing. It experiences a non-negligible vertical extension of roughness elements including stones, vegetation, trees and buildings. This lowest layer is also called the roughness sub layer. The upper part of the surface layer is called the inertial sub layer as shown in figure 2.1. The figure shows that in cases of relatively smooth surface like short grass or sand the inertial sub layer will be associated with the entire surface layer since the roughness sub layer is significantly reduce becoming very thin.

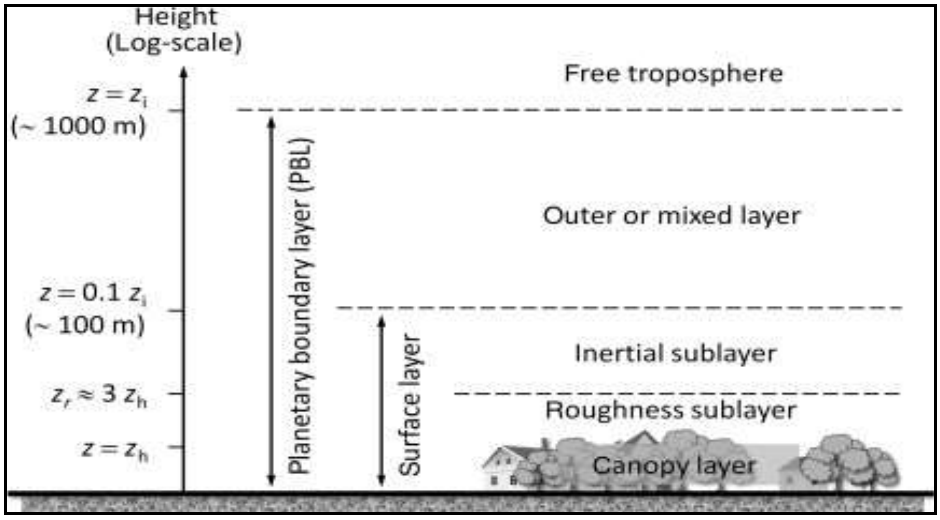

Figure 2.1: Conceptual representation of the surface layer in the PBL

The flow in the roughness sub layer is three dimensional in nature due to the effects of roughness elements. Horizontal variability brought about by roughness elements vanish at the upper boundary, z_r making the flow horizontally homogeneous. The depth of the roughness sublayer varies depending on the height of the roughness elements. Urban environments fall within this sublayer where buildings and other infrastructure largely create the rough surfaces, creating fluctuations in speed and direction. Harnessing wind power within this environments presents a complex mathematical analysis for predicting turbine power output. The free atmosphere comes above the PBL where the wind is approximately geostrophic, flowing parallel to the isobars and unaffected by surface drag (Manwell *et al*., 2009).

2.2.6 Boundary layer behaviour on surfaces

The interaction of the fluid with the surface of the object as the object moves through a fluid or a fluid moves over the object causes disturbance to the flow of the molecules. A drag force element results from the pressure distribution over the aerofoil and the friction between the flowing air and the aerofoil. This is highly dependent on the

viscosity of the fluid. This drag interaction leads to two distinct regions of flow; one further from the surface of the aerofoil where the friction forces are not significant and another immediately next to the surface, dominated by friction forces, called the boundary layer. As the fluid flows over the surface, molecules that are next to the surface stick to the surface. The sticking molecules then slow down those just above the surface as they collide. The velocity will thus increase as one moves away from the surface because of fewer collisions. A boundary layer is then created close to the surface where the velocity changes from zero and increases upwards to the free stream flow away from the surface (John & Anthony, 2006).

Reynolds number also determines whether a boundary layer is laminar or turbulent. In a laminar boundary the fluid molecules close to the surface slow down and appear to have zero velocity because of fluid viscosity creating drag on the particles above them. In turbulent boundary layer, very large eddies form that are sometimes larger than the molecules. Slower eddies closer to the surface mix up with faster moving air masses above the surface causing the turbulent layer to move faster than the laminar layer at the same characteristics. The drag is higher in turbulent flows and they are less susceptible to flow separation. These characteristics on the boundary of surfaces can be manipulated and modified to optimize performance of aerofoils (Gagliano *et al*., 2013).

2.2.7 Reynolds Number

Reynolds number, Re, is dimensionless parameter expressing the ratio of inertial forces (resistance to motion or change) to viscous forces. This parameter is important in determining whether a flow will be laminar or turbulent. Equation 2.12 is the expression of Reynolds number:

$$\mathrm{Re} = \frac{\rho V D}{\mu} = \frac{VD}{v} \quad \text{......} \quad 2.12$$

where; V is the velocity, D is the characteristic linear dimension or length of fluid travelled, ρ is the density of the fluid, μ is the dynamic viscosity and v the kinematic viscosity. figure 2.2 shows an illustration of behaviour of molecules in a flow field for either laminar or turbulent flow due to Reynolds number.

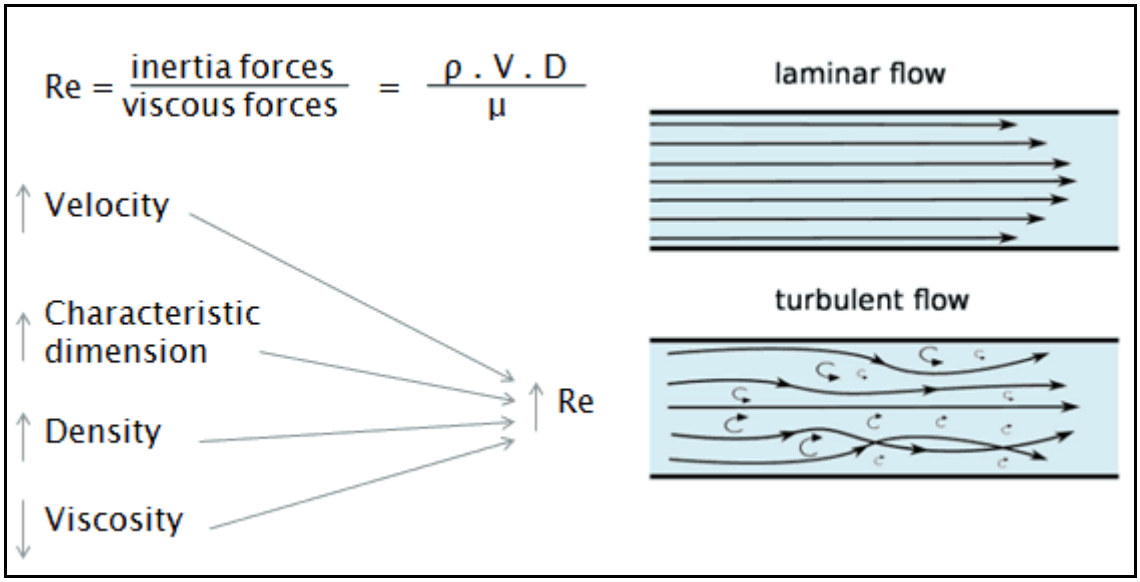

Figure 2.2: Illustration of laminar and turbulent flow due to Reynolds number

When the viscous forces are dominant meaning that the flow is slow and Reynolds number is low the fluid particles will be kept in line and thus the flow is classified as laminar. On the other hand, when inertial forces are dominant and the fluid is flowing faster the Reynolds number is large and the flow characterized as turbulent. Laminar flows are observed when the Reynolds number is less than 2000 while turbulent flows are observed at Reynolds number above 3500. In between there is the onset of turbulence a phase known as transitional flow where the fluid flow changes from laminar to turbulent. Laminar flow has low velocity and fluid particles move in straight lines. The layers of the fluid flow over one another without mixing. Laminar flow is

rare and can be analysed using simple mathematical methods. Turbulent flow on the other hand moves at high velocity with irregular movement of the particles of the fluid. It is the most common flow type requiring very difficult mathematical methods to analyse. Characterizing fluid flow due to Reynolds number is very important in evaluating performance of turbines that operate predominantly within these conditions (Wekesa *et al*., 2017).

2.2.8 Wind in urban and built environments

Urban environments are associated with turbulent winds because of enhanced local roughness, and by virtue of their low location in the planetary boundary layer. These results to complex, gusty, and shifting urban wind resource exhibited by relatively rapid changes in both wind direction and magnitude. Wind turbines operate almost exclusively within the lower 10% of the earth's planetary boundary layer in a region termed the internal sub-layer (McIntosh, 2009, Wekesa *et al*., 2017). Turbine aerodynamics requires the study of the wind resource at typical turbine heights which sits within the larger framework of meteorology and the study of the planetary boundary layer depicted by a mean velocity profile in figure 2.3.

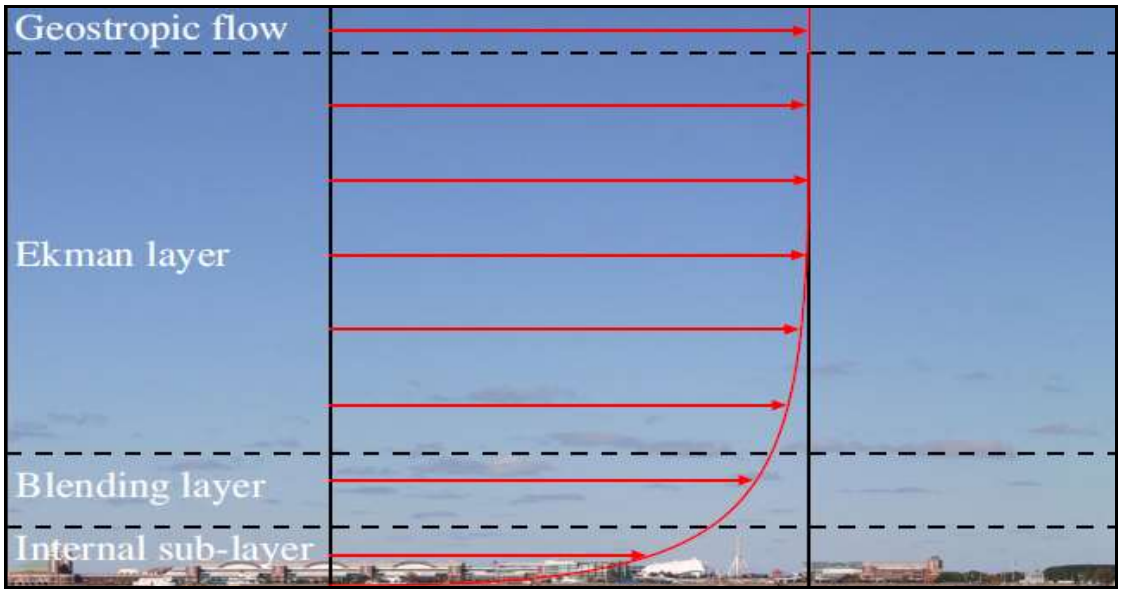

Figure 2.3: A typical planetary boundary layer's mean velocity profile (McIntosh, 2008)

The measure of mean wind speed and its fluctuations, wind's 'gustiness,' are the most important factors that control the amount of energy available to a turbine and the ability of the turbine to extract useful work. Unsteadiness within the internal sub-layer, characterized by amplitude fluctuations causes a departure of wind speeds away from the long term mean to span a vast range of time scales ranging from months to seconds (McIntosh, Babinsky & Bertenyi, 2007):

$$\mu(t) = \bar{\mu} + \mu'(t) \quad \text{.....2.13}$$

where μ is the fluctuating wind as a function of time, t, $\bar{u}$ is overall mean wind speed and μ' is the fluctuations from the wind speeds.

Consequently, a much more detailed assessment of unsteadiness lying within the short period range is necessary to inform the design and optimization of wind turbines operating within this unsteady environment. It is worth noting that the term gustiness is frequently used to describe these short period fluctuations, generated by atmospheric

instabilities (buoyancy terms) and the mechanical shear (kinetic terms). Therefore, an assessment of the wind resource can be analyzed out by splitting unsteady wind into three components expressed in equation 2.14 (Wekesa *et al*., 2017):

$$\mu(t) = \bar{\mu} + \mu'_{sp}(t) + \mu'_{lp}(t) \quad \text{.....2.14}$$

where $\bar{\mu}$ is overall mean wind speed, u'_{sp} is short period fluctuations in the order of seconds to minutes, and u'_{lp} is long period fluctuations in the order of 10 to 100 hours.

2.2.9 Urban wind resource in a turbulent context

Urban winds are characterized as having low wind speeds with more turbulent flow that results in limited energy realization (Sunderland *et al.,* 2015). Air flowing across an urban area becomes affected by its characteristics on interacting with the underlying urban subtype (Wekesa *et al*., 2016). There exist three atmospheric stability classifications namely unstable, stable, and neutral. Figure 2.4 illustrates a description of the wind speed in the direction of the air flow within a boundary layer where air flow was adjusted to the underlying surface (Sunderland *et al*., 2015).

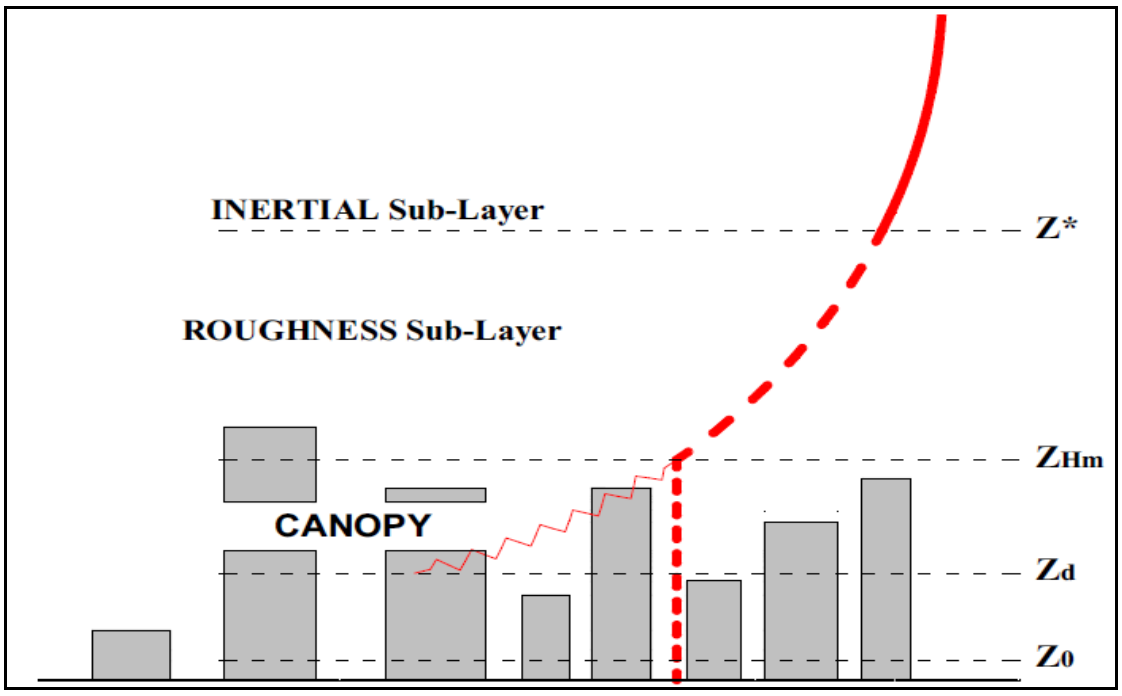

Figure 2.4: Urban air-flow model in terms of the logarithmic model (Sunderland et al., 2015)

The velocity scale representing this shear stress within internal-boundary-layer, termed by the frictional velocity u_f is defined by equation 2.15 (Wekesa *et al*., 2016):

$$u_f = \left[\frac{\sigma_w}{\rho}\right]^{\frac{1}{2}} \quad \text{.....2.15}$$

where; ρ is the density of the air flow within internal boundary layer.

The rate of strain within the internal sub-layer has been dimensionally argued to be proportional to the ratio of frictional velocity and height in equation 2.16 (Wekesa *et al*., 2016):

$$\frac{\partial u}{\partial z} \propto \frac{u_f}{z} \quad \text{.....2.16}$$

Therefore, urban wind turbines (composed of vertical axis wind turbines, VAWTs) are sited in areas of high terrain roughness and need to be able to respond to short-period micrometeorological fluctuations accurately due to the meaningful energy content at these scales (Bertenyi, Wickins & McIntosh, 2010)

Integrating equation 2.16 yields an expression for the mean wind speed as a function of height (z) above the ground termed log-law which is the similar to equation 2.1, and a parameter termed the surface roughness height, z_0, equation 2.17:

$$\bar{u}(z) = \frac{u}{k}\ln\left(\frac{z}{z_o}\right) \quad \text{.....2.17}$$

defining the frictional velocity u_f (shear velocity) as equation 2.18 (Wekesa *et al*, 2016):

$$u_f = \frac{k\bar{u}}{\ln\frac{z}{z_o}} \quad \text{.....2.18}$$

where k is Von Karman's constant. The frictional velocity u_f is measure of the shearing stress that drives the flux of momentum to the Earth's surface (Figure 2.4). It is properly applied to extensive homogeneous surfaces (like grass) under neutral atmospheric conditions and is valid under the circumstances to heights above the ground ($z_o + z_d$), where at z_o the displacement height identifies the level of aerodynamic surface where $u(z)$ goes to zero (Bertenyi *et al*., 2010).

2.2.10 Changeability and gustiness

McIntosh *et al*., (2008) proposed a notation to describe unsteady wind variations experienced by a wind turbine rotor axis during a gust, expressed as:

$$D_g = \frac{U_{mean}}{f_c} \quad \text{..... 2.19}$$

where; D_g is the gust length, U_{mean} is the mean speed of unsteady wind, and f_c is the characteristic fluctuation frequency of the gust. The gust-induced unsteady aerodynamic effects can then be characterized by a reduced gust frequency relating the rotor's radius R_{rotor} to the characteristic frequency f_c of the fluctuating wind, expressed as in equation 2.20 (McIntosh, 2008):

$$k_{gust} = \frac{2R_{rotor}}{D_g} = \frac{2R_{rotor} f_c}{U_{mean}} \quad \text{..... 2.20}$$

following the notation by Wekesa *et al*., (2014) the number of rotor revolutions per one full cycle of wind fluctuation, n_{turb} can be expressed as in equation 2.21.

$$n_{rev} = \frac{\lambda_{mean}}{\pi k_{gust}} = \frac{\lambda_{mean} U_{mean}}{2\pi R_{rotor} f_c} \quad \text{.....2.21}$$

where the mean tip speed ratio $\lambda_{mean} = (\omega_{mean} R_{rotor})/U_{mean}$. Total available energy in wind E_{wind} over period of operation T can be calculated through an integration of available wind power using the equation 2.22 (McIntosh, 2008):

$$E_{wind} = \frac{1}{2}\rho A \int_0^T U_\infty{}^3(t)dt \quad \text{..... 2.22}$$

Consequently, the ratio of extracted aerodynamic energy $E_{turbine}$ to available wind energy over a predefined period of time yields the energy coefficient C_e (McIntosh, 2008):

$$C_e = \frac{E_{turbine}}{E_{wind}} = \frac{\int_0^T Cp(\lambda) U_\infty^3(t) dt}{\int_0^T U_\infty^3(t) dt} \quad \text{..... 2.23}$$

where C_P is the power coefficient as function of λ evaluated over one fluctuation wind cycle.

2.2.11 Turbulence and turbulence intensity

Turbulence is fluctuation in the wind flow. Turbulence is associated with random and continuously changing direction and velocity in fluids. These changes in wind flow are usually associated with gusts superimposed on the wind's average direction. Steady flow means low turbulence while unsteady flow will have high turbulence. Turbulence is an important element in wind power production since it impacts turbine loading, fatigue, wake effects and performance effects. In the planetary boundary layer turbulence is as a result of friction and interaction of air with the earth surface and obstacles. Convective turbulence is also generated from thermal heating of the earth. Trees, buildings and other infrastructure close to the ground also result to turbulence. Turbulence in the Atmospheric Boundary Layer (ABL) results to fluctuations in both wind speed and direction which are key factors in wind turbine siting and blade design for efficient power production (Lubitz, 2014, Wekesa *et al*., 2017). While turbulence is usually unpredictable, there are aspects that can be analysed statistically and power performance of wind turbines predicted.

In wind energy industry, turbulence is quantified with a metric called turbulence intensity; which is the standard deviation of the horizontal wind speed divided by the average wind speed over some time period say 10 minutes. Turbulence intensity (TI) is a uniform measurement scale of whether turbulence is high or low. It is a scale

characterizing turbulence expressed as a percentage. Idealized flow with no turbulence would have a TI value of 0%.

In this study, a Pitot-static pressure probe was traversed through different positions in an empty tunnel test section, which is the position of the centre of the VAWT rotor to find the real reference wind speed. The turbulence intensity at the wind tunnel test section in the absence of turbine was be determined by the equation (Wekesa *et al.*, 2016):

$$TI(\%) = \frac{\mu_{rms}}{\overline{U}} \times 100 \quad \text{.....2.24}$$

where $\overline{U}$ is the time averaged value of the stream-wise velocity signal and μ_{rms} is the root mean square of the velocity fluctuations in the stream-wise direction, calculated from (Kaldellis *et al*., 2011):

$$\mu_{rms} = \sqrt{\frac{1}{n-1}\sum_{i=1}^{n}\left(u_i - \overline{u}\right)^2} \quad \text{..... 2.25}$$

where n is the sample number in velocity signals and u_i is the stream-wise velocity component for individual velocity signal.

Turbulence intensity can increase mechanical stress on turbine components and reduce fatigue life for the turbine structure (Lubitz, 2014). Areas with very uneven terrain surface and behind obstacles such as buildings have a lot of turbulence with very irregular wind flows, often in whirls (Wagner & Mathur, 2012). This decreases the possibility of using energy in wind effectively for a wind turbine and imposes more wear and tear on the wind turbine. Equally, local turbulence and complex terrain may mean that wind gusts hit the rotor from varying directions. This introduces a difficulty in reproducing performance power curves for same turbines under different conditions. However, with research and characterization of the behavior of wind over surfaces in

turbulent conditions, rotor models can be designed to operate within these conditions and maximize the periods of high energy in the gusts for wind energy production. This requires an understanding of airfoil aerodynamics and the collective performance of rotors in non-uniform wind regimes.

2.2.12 Aerodynamics of aerofoils for wind turbines

Wind is harnessed using wind turbines. These turbines as earlier discussed are created from aerofoils that interact with wind causing mechanical power to be converted to electricity. Aerofoils are cross sectional shapes of a wing, blade or sail with specific geometric shapes that are used to generate mechanical forces due to their relative motion as they cut through a surrounding fluid. These structures are used in wind turbines to generate mechanical power. Cross-sections of wind turbine blades are designed with an aerofoil shape as shown in the figure 2.5. The selection of width and length depend on the intended aerodynamic performance, maximum expected rotor power, and properties of the specific aerofoil and the strength of the structure.

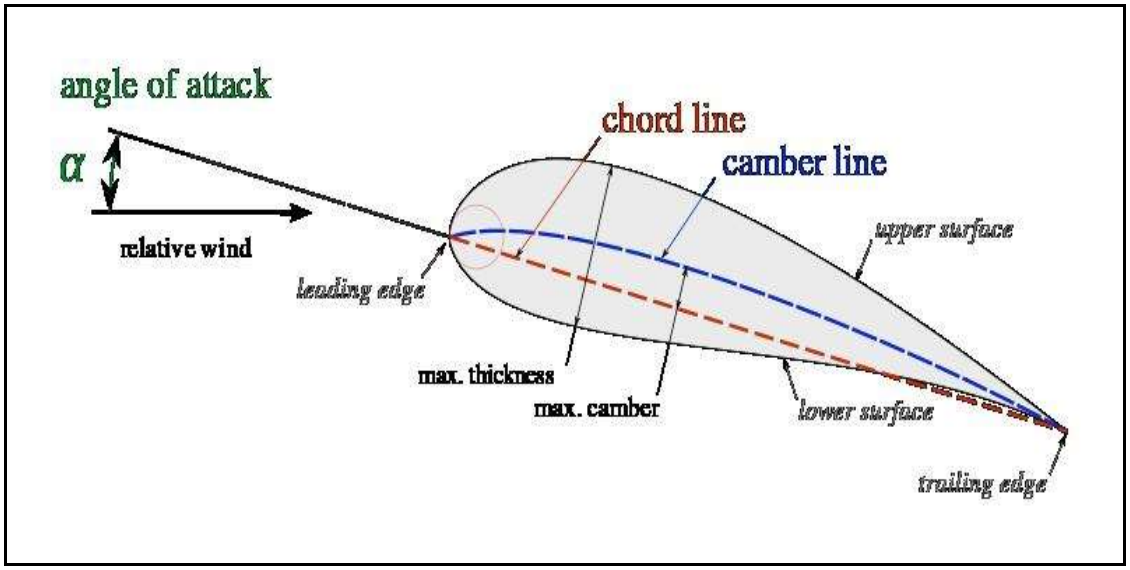

Figure 2.5: Aerofoil profile and properties

The different parts of the aerofoil contribute to the overall process of lift generation. The mean camber line is the locus of points halfway between the upper and lower surfaces of the aerofoil. The leading and trailing edge are the most forward and rearward points of the structure on the mean camber line, respectively. Chord line is a straight line that connects the leading and trailing edge. Chord, c is the distance from the leading to the trailing edge along the chord line. Camber is the distance between the mean camber line and the chord line measured perpendicular to the chord line. Thickness is the distance between the upper and lower surfaces measured perpendicular to the chord line and angle of attack, is the angle between the relative wind/airflow and the chord line of the aerofoil.

These characteristics affect the aerodynamic performance of the turbine developed. This research work used the symmetric NACA 0012 profile that has 12% thickness. These profiles interact with the airflow and result to movement through balancing of different forces acting on them including lift, drag, thrust and weight.

When the air flows over an aerofoil there is a distribution of forces over the surface. The flow velocity over the aerofoils increases over the convex surfaces resulting in lower average pressure on the suction side of the aerofoil compared with the concave or pressure side of the structure. Meanwhile, viscous friction between the air and the aerofoil surface slows the air flow to some extent next to the surface. These behaviour of a fluid in the immediate vicinity of the bounding surface is discussed as boundary layer conditions with governing equations for turbulent conditions detailed later in this thesis.

Due to these actions, the resultant effect is resolved to drag and lift force and a moment that acts along the a quarter chord distance from the leading edge:

Lift force: The force acting perpendicular to the direction of the incoming airflow that is as a result of unequal pressure on the upper and lower aerofoil surfaces.

Drag force: Force parallel to the direction of incoming airflow that is as a result of viscous friction forces at the surface of the aerofoil and unequal pressure on the aerofoil surface facing toward and away from the incoming flow.

Pitch moment: The moment about an axis perpendicular to the aerofoil cross section

The following two-dimensional coefficients are important in rotor designs and performance: lift coefficient:

$$C_l = \frac{L/l}{\frac{1}{2}\rho U^2 c} = \frac{Liftforce/unitlength}{Dynamicforce/Unitlength} \quad \ldots\ldots 2.26$$

two dimensional drag coefficient;

$$C_d = \frac{D/l}{\frac{1}{2}\rho U^2 c} = \frac{Dragforce/unitlength}{Dynamicforce/unitlength} \quad \ldots\ldots 2.27$$

and the pitching moment coefficient as;

$$C_m = \frac{M}{\frac{1}{2}\rho U^2 Ac} = \frac{Pitchingmoment}{Dynamicmoment} \quad \ldots\ldots 2.28$$

Where, ρ is the density of air, U is the velocity of undisturbed air flow, A is the projected aerofoil area (chord span), c is the aerofoil chord length and l is the aerofoil span. These dimensionless parameters are important in analysing wind turbine performance.

Resultant lift on the surface of an aerofoil is due to the balancing of pressure. The curved part of the wing lowers the pressure directly above it causing it to move upwards. When the air flows over the curved upper surface it is inclined to move in a

straight line. However, the curves in the wings pulls it around and backward effectively stretching it out into a bigger volume. This forces some of the molecules to occupy a bigger volume and results to lower pressure. On the other hand, the lower surface squashes molecules into a smaller space thus higher pressure. As a result a pressure difference is created causing lift. The more an aerofoil splits/diverts the path of incoming air, the more lift is generated. This thesis uses a symmetric profile where the upper surface is same as the lower surface. The angle of attack creates a situation where the aerofoil interacts with air and causes it to split accordingly creating lift.

2.2.13 Power Curve of Wind Turbine

This is a curve that shows how power output from a wind turbine relates to steady wind flow as shown in figure 2.6.

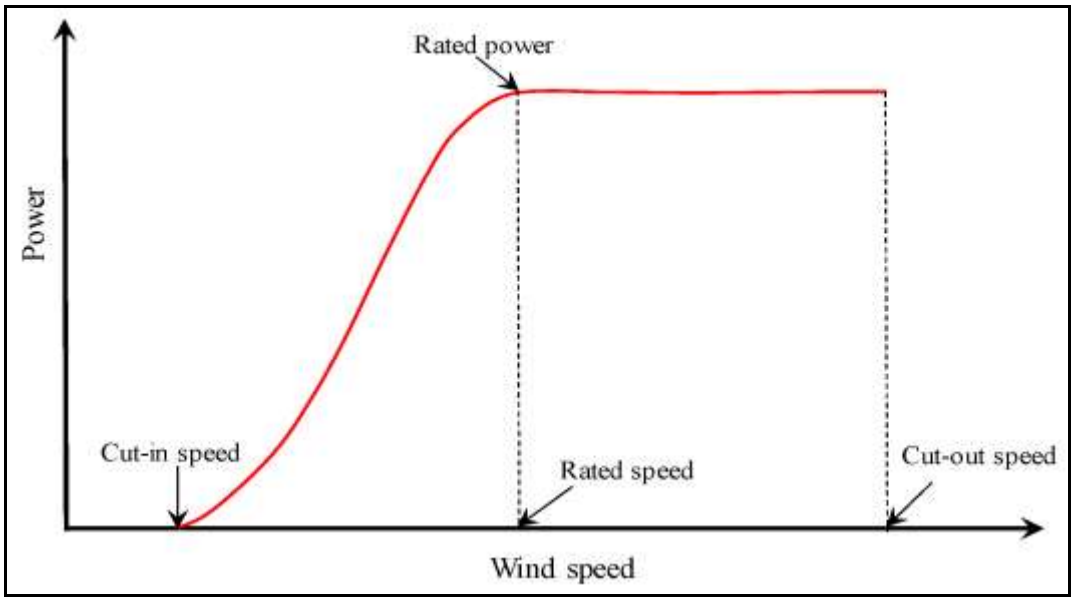

Figure 2.6: Typical wind power output versus steady wind speed

The characteristics of the power curve are defined as follows:

Cut-in speed: This is the speed at which the turbine will begin to generate power. The blades are not able to rotate at low wind speeds because insufficient torque is exerted on

the rotor. The wind speed continues to increase and generate more torque up to cut-in speed where power generation begins. Different turbines have different cut-in wind speeds.

Rated power and speed: Above the cut-in speed the electrical power increases rapidly with increasing wind speed until it comes to the limit for the specific turbine and electric generator. This power is called the rated power and the speed at which is obtained known as the rated speed. Each turbine design has a recommended rated power and speed. Different mechanisms are instilled within turbines to maintain this rated power output even at higher speeds.

Cut-out speed: With increasing speed, associated forces on the turbine also increase causing a risk of damage to the rotor. This usually requires a braking system to stop the system. The speed at which this is done is called the cut-out speed.

2.2.14 VAWT rotor flow governing equations

Performance of a rotor and prediction of induced velocity field are important aspects of rotor aerodynamics. Analysis of a rotor with respect to its geometry and operating conditions is done by solving partial differential equations as governing equations describing conservation of mass, momentum and energy. Conservation of mass equation is important in determining if a flow field is possible or not.

Flow near a VAWT is represented by incompressible Navier-stokes equations. These are derived from an idealized incompressible flow. The continuity equation and conservation of momentum equations for the incompressible flow are:

$$\frac{\partial u_i}{\partial x_i} = 0 \quad \text{..... 2.29}$$

$$\rho \frac{\partial u_i}{\partial t} + \rho u_j \frac{\partial u_i}{\partial x_j} = -\frac{\partial p}{\partial x_i} + \frac{\partial \tau_{ij}}{\partial x_j} \quad \text{..... .....} \quad 2.30$$

where; i, j = 1, 2, 3. x_1 and x_2 denote horizontal and vertical positions, respectively; u_i and u_j are the corresponding mean velocity components; t is time; ρ is the density of the fluid; p is the dynamic pressure; and τ_{ij} is the viscous stress tensor defined by:

$$\tau_{ij} = 2\mu s_{ij} \quad \text{.....2.31}$$

where μ is the molecular viscosity and s_{ij} is the strain-rate tensor obtained from the equation :

$$s_{ij} = \frac{1}{2}\left(\frac{\partial u_i}{\partial x_j} + \frac{\partial u_j}{\partial x}\right) \quad \text{..... 2.32}$$

rewriting and simplifying equation 2.30 yields the Navier-Stokes equation in conservation form:

$$\rho\frac{\partial u_i}{\partial t} + \rho\frac{\partial u_i . u_j}{\partial x_j} = -\frac{\partial p}{\partial x_i} + \frac{\partial}{\partial x_j}\left(2\mu s_{ij}\right) \quad \text{..... 2.33}$$

time averaging equation 2.33 yields the Reynolds averaged equations for motion in conservation form defined by:

$$\rho\frac{\partial u_i}{\partial t} + \rho\frac{\partial u_i . u_j}{\partial x_j} = -\frac{\partial p}{\partial x_i} + \frac{\partial}{\partial x_j}\left(2\mu s_{ij} - \rho\overline{u'_j\, u_i'}\right) \quad \text{..... 2.34}$$

where $\overline{u'_j u'_i}$ is the Reynolds stress component where u'_i denotes the fluctuating part of the velocity. Substituting equation 2.32 into equation 2.34 yields its most recognizable form of Navier-stokes equation given as:

$$\rho\frac{\partial u_i}{\partial t} + \rho\frac{\partial u_i . u_j}{\partial x_j} = -\frac{\partial p}{\partial x_i} + \mu\frac{\partial^2 u_i}{\partial x_j \partial x_j} - \rho\frac{\partial \overline{u'_j u_i^i}}{\partial x_j} \quad \text{..... 2.35}$$

with the kinematic viscosity value as

$$\nu = \frac{\mu}{\rho} \quad \text{2.36}$$

hence applying Reynolds decomposition and taking the time average of the continuity momentum equation 2.29 and equation 2.36 yields the unsteady RANS equations for incompressible flows in differential form:

$$\frac{\partial u_i}{\partial x_i} = 0 \quad \text{2.37}$$

$$\frac{\partial u_i}{\partial t} + u_j \frac{\partial u_i}{\partial x_j} = -\frac{1}{\rho}\frac{\partial p}{\partial x_i} + \nu \frac{\partial^2 u_i}{\partial x_j \partial x_j} - \frac{\partial \overline{u_j' u_i'}}{\partial x_j} + f_i \quad \text{2.38}$$

where the term $f_i = \rho\vec{g} + \vec{F}$ represents other body forces commonly referred to as forces per unit volume such as gravity and centrifugal forces. This forces will be ignored in this study for simplicity. The left hand side of equation 2.38 corresponds to the change in mean momentum of the fluid element due to unsteadiness in the mean flow and its convection. The resulting change is balanced by the mean body force, the isotropic stress due to the mean pressure field, the viscous stress and apparent stress due to fluctuating velocity field generally termed as Reynolds stress $\left(-\overline{u_j' u_i'}\right)$. The Reynolds stress are initiated by fluctuations associated with turbulence.

2.3 Previous works relevant to study

Research into the design, development and performance of VAWT for optimization of power output has been ongoing since the 1970's especially by the Sandia National Laboratory of the USA Department of Energy. Research has applied both numerical and experimental approaches which have continually developed through mathematical models to experimental methods and currently applying computational models. The

design process of VAWT has largely been improved by the understanding of geometric properties of VAWT and their behavior under different conditions, (Danao *et al*., 2013). This section presents the numerous efforts made to understand the individual parameters of a VAWT and the complicated process of power production due to their interaction with different wind conditions.

Aerodynamic performance data on symmetric airfoils have been available for a long time making them more preferable choice of airfoil. Jacobs and Sherman (1937) investigated the performance of NACA airfoils to characterize their behavior at different values of Reynolds number. They systematically investigated representative groups of NACA airfoil through a range of Reynolds numbers focusing on statistical tests of lift and drag (Jacobs and Sherman, 1937). A study by Healy, (1978) used the dataset from this research to analyze the effects of camber and thickness on the performance of a VAWT by developing a model for the vertical axis wind turbine. The study concluded that thicker airfoils performed better at lower Reynolds number which they attributed to their resistance to stall, (Healy, 1978, Danao *et al*., 2013). Danao et al., (2013) conducted CFD study of camber and thickness and disputed this result. They observed that thinner airfoils produced higher amounts of lift when subjected to stronger pressure gradients. Further, Healy, (1978) from a camber analysis study, suggested that it had a negative effect on performance and proposed that symmetric profiles would be more efficient. In their analysis of the performance of cambered airfoils, Baker, (1993) and Kirke (1998) found that cambered or angled blades increased performance in especially in the upwind and would be more beneficial for power production. The study argued that cambering also improved the self-starting ability of a turbine by shifting the performance curve to the left in regions of lower tip speed ratio, (Baker, 1993, Kirke 1998). Due to separation occurring at lower Reynolds number and occurrence of early flow separation prior to stalling, Danao *et al*., 2013 suggested that to maximize output, a leading edge should be cambered and the nose rounded, (Danao *et al*., 2013).

McIntosh (2009) compared the performance of thinner airfoils to thicker airfoils and concludes that higher maximum CP was registered for thinner airfoils than thicker airfoils. The thinner airfoils register a sharp drop in CP from the maximum value while a gentler rounded top of the CP for thicker airfoils suggest that the change is not as drastic. It is further shown that the maximum CP shifts to lower tip speed ratio values for thicker airfoils. This behavior makes thicker airfoils more suited for gusty wind environments where the fluctuations in tip speed ratio is small CP doesn't drop much. 2D CFD simulations performed by Danao *et al*., (2013) on several airfoil profiles to study the effect of camber and thickness showed that a higher maximum CP is obtained from thinner symmetric sections while cambering of thick profiles register an overall improvement in performance, (Danao *et al*., 2013).

Power performance of a VAWT cannot only be attributed to specific components of the turbine, rather all the parameters are interlinked to give an output. The studies above present the effect of these constituent elements to the performance of a turbine. Research into the effects of non-uniform wind on the performance of vertical axis wind turbine is a recent event with little existing literature on the same. Numerical models have been used before. Turbulence intensity is the metric used to quantify and characterize levels of non-uniform wind. It is a complex process that has significant effect on the power produced, nature of power curves and efficiency of the turbines. This is particularly crucial for small wind turbines which in practice are typically installed near buildings, trees, and other obstacles, (McIntosh, Babinsky & Bertenyi, 2008, Lubitz, 2014).

Smith, (2010), described performance curves and annual energy production for seven different wind turbines subjected to different turbulence intensities. The study reported that the turbines' annual energy production varied from 9% to 32% over the range of turbulence intensities that were used. The energy produced by most turbines was low in both cases of very low and very high turbulence intensities, apart from one that showed increased annual energy production with increasing turbulence levels.

The study in Lubitz, (2014) investigated the effect of ambient turbulence levels on wind turbine energy production. They used a Bergey XL 1 small wind turbine in an open field environment. The turbine was a horizontal axis wind turbine with rated power of 1 Kw, 24 V consisting three blades of 2.5 m in diameter. The turbine was installed on an 18 m tower in an open field and the power output dissipated and measured across a dynamic braking resistor rated 2180 W, 2 Ω. The turbine was located in a representative open field environment largely away from buildings, trees and other obstacles. The main objective of the study was to find out how the ambient turbulence would affect the behavior of a wind turbine. The study did not use data from sectors that were considered disturbed so as to keep the results as general as possible and not to include wake effects from individual buildings and other obstacles in the analysis. Cut-in wind speeds of 4 m/s were recorded with cut-out speeds and furling experienced at 9 m/s. Based on the turbulence intensity, the data was divided into three: low turbulence (intensity < 0.14), high turbulence (intensity > 0.18) and intermediate turbulence (between 0.14 and 0.18). This study concluded that low turbulence resulted to a decrease in power production while intermediate and high turbulence, within the operating range of 4 m/s to 7 m/s, resulted to a significant increase in power production. However, at wind speeds associated with furling events, low turbulence was observed to cause an increase in power produced. Ambient turbulence intensity has an effect on the energy produced but the impact varies with different turbine characteristics. Lubitz, 2014 argues that the performance of wind turbines in urban environments is subject to the intensity of turbulence and the size of the turbulence scales.

Kooiman and Tullis, (2012) conducted a study on how rapid fluctuations in wind direction and velocity within urban environments affects the power production characteristics of a VAWT. The study placed 3 bladed H-type Darrieus VAWT, of diameter 2.5 m and 3 m height on a rooftop of an industrial building (20 m by 80 m by 40 m) in a built environment. The turbine was at the centre of the building and positioned 4.5 m above it. Power was extracted and quantified using an electrohydraulic disk brake system which measured the load imposed tangentially to the rotation of the

turbine. They observed that power production varied with fluctuating wind velocity but not much change was observed when the wind direction changed. This behavior on the urban tested turbine was then compared to results from the same turbine that was performed in a wind tunnel with low turbulence (of TI less than 2%) as a benchmark for the performance. They observed a marginal reduction in the turbine's power performance from the smooth flow values for TI less than 15% and almost a linear power reduction with increasing wind velocity fluctuations and turbulence greater than 15%, (Kooiman & Tullis, 2012). The study concluded that with considerations of appropriate site characteristics, performance degradation can be minimized and VAWT used conveniently within urban environments.

The studies by Smith, (2010), Kooiman and Tullis, (2012) and Lubitz, (2014) were all conducted in open atmospheric environments. The researchers did not have a control on the levels of turbulence the turbines were subjected to. To determine the turbulence intensities, the data was divided into small sections and turbulence intensity calculated from the variance of each section. These studies then compared the behavior of the turbines in each data section so as to characterize and quantify how they are affected by the wind turbulence. This procedure is largely dependent on the sample size of each data section and the prevailing atmospheric wind conditions that vary due to different time scales such that using a different data size at different times may give a totally different result and characterization of the effect of turbulence on the wind turbine.

Considering the said limitations, Mojtaba *et al*. (2015) performed a study on the performance of a VAWT in a turbulent environment. In this study, a five-blade commercial mini-VAWT was tested in a closed loop wind tunnel environment. Turbulence intensity levels of 5%, 7.5% and 10% were generated in the tunnel by positioning the turbulence generator in three different locations upstream of the wind turbine, (Mojtaba *et al.*, 2015). They measured the output power was measured by tracking the voltage across an external load having an electrical resistance of equivalence 153 Ω. Rotational speeds greater than 300 RPM were measured using a digital stroboscope while those below 300 RPM were recorded on a high performance

camera rated 60 fps. This study reported the turbulence characteristics in form of stream-wise velocity fluctuations, probability density function and frequency spectra. They observed an increase in the voltage as turbulence intensity jumped to 5%, 7.5% and 10% as compared to the smooth flow case of 0.5%. This behavior was attributed to the fundamental change in the underlying flow regime around the blades from laminar flow to turbulent flow. It was also reported that the self-starting capabilities of the turbine improved with the turbine starting at 3 m/s at turbulence intensity of 5% compared to the smooth flow conditions of 0.5% where self-starting was observed at 3.5 m/s. This study created quasi-isotropic turbulent winds but was limited to lower tip speed ratios below 1 (Mojtaba *et al*., 2015). It is interesting to study and observe the behavior of a VAWT subjected to tip speed ratios above 1 in a wind tunnel environment.

Pagnini, Burlando and Repetto, (2015) performed an experimental analysis of two small-sized wind turbines (HAWT and VAWT) with the same rated power, 20 kW and operated in the same urban environment. The turbines were located at a harbor which was characterized by two distinct wind regimes of low turbulence from wind blowing from the sea and high turbulence from wind blowing from land. They used a three-bladed HAWT of diameter 10 m with an active yaw mechanism and a synchronous generator (supported by 18 m high pole). The VAWT on the other hand was a five-bladed H-rotor turbine of diameter 8m and 5.8 m height (supported by 10.5 m high pole). The turbines were installed on a dam 4.5 m high and a monitoring system registered and collected data at a sampling rate of 10 s (Pagnini *et al.,* 2015). The study concluded that the HAWT had a higher overall energy production than the VAWT though it is affected more by the fluctuations in wind mean velocity and direction. The VAWT on the other hand is less exposed to gusts and fluctuations in wind directions and that was actually able to operate at higher wind velocities improving the overall efficiency of the system (Pagnini *et al*., 2015). In the moments that the wind blows from the sea (low turbulence) the HAWT is observably higher than the VAWT while in the high turbulent moments when the wind is blowing from the land the VAWT is seen to

register higher power. Pagnini et al., 2015 concluded that the VAWT shows better technical and operational capability in more turbulent conditions as compared to the HAWT. The study suggested that both turbines were still not adequate for deployment in complex environments due to their high sensitivity. Different levels of turbulence affect a turbine differently. This study only compares the horizontal and vertical axis turbine behaviors with no information on how different turbulence levels would affect the aerodynamic characteristic of the turbines.

Sunderland, Woolmington and Blockledge, (2015) in their study presented two models that could be used to study the variations in wind speeds over a considerable time interval and how this affects the wind turbines. The first model is a Gaussian probability distribution that was largely derived to quantify the degradation in power performance among wind turbines on a wind farm. The second model used was the Weibull distribution which is a common probabilistic method of describing wind speeds. The study adopted a power curve for a 2.5 kW wind turbine that showed how the turbine is affected by varying turbulence as a reference that was compared with observations by the two models. A sonic anemometer was positioned 1.5 m above buildings in two representative sites in the urban environment. Estimation was done for turbulence in form of turbulence intensity using the two models and the behavior as predicted by the two models compared to the industrial power curve given for the adopted wind turbine. Sunderland *et al*., (2015) reported that the two models were within a 0.2% error range of the adopted power curve. Gaussian statistics and Weibull distribution can be used to predict the effect of turbulence on the power production of a wind turbine in an urban environment.

Chong, Fazlizan, Poh, Pan, Hew and Hsiao (2013), designed and analyzed an Omni-direction-guide-vane (ODGV) around a VAWT in order to improve its performance. The study tested a 5-bladed H-rotor wind turbine in a wind tunnel with and without the integration of the ODGV (Chong *et al*., 2013). The vane was designed to capture wind from all direction, guide the wind to an optimum angle of attack and increase the speed due to Venturi effect. This study reported that with the speed increased and direction

controlled the self-staring ability of the turbine was improved with the turbine self-starting at 4 m/s in the presence of the ODGV over the 7.35 m/s without the guide vanes. Further, the rotational speed and power output were significantly improved by 182% and 3.48 times respectively in the presence of the ODGV.

Wekesa *et al*., (2016) presented an experimental method for deeper understanding of the unsteady rotor aerodynamics under turbulent flow operating conditions. The study developed and tested a small scale Savonius turbine in a wind tunnel. They reported that the results obtained from experiment showed that power production by wedge generated turbulent flow was slightly higher than that produced by uniform flow, though drastic reduction was evident at wind speeds above 7 m/s. The study also showed a dual influence of turbulence intensity on the small wind turbines. Presence of turbulence inflow increased the kinetic energy available to small wind turbines at low wind speeds and also tends to increase efficiency at wind speeds near furling speed. It was also noted that the self-starting ability of the VAWT was improved on introducing an external turbulent inflow. This was attributed to the reduction of the relative velocity between approaching wind and rotor at low tip speed ratios, which resulted in a lower moment that decays rapidly as the turbine starts rotating (Wekesa *et al*., 2016).

It can be seen from literature that most of the recent research had been done in open environments where there was little control on the free-stream turbulence characteristics. Using the same methodology to quantify the effect of the turbulence makes it highly dependent on the sample size. Lubitz (2014) observes that the interaction of small wind turbines with wind is a complex process and highly dependent on the characteristics of the wind turbine. The work by Wekesa *et al*., (2016) only observed the behavior of a Savonius type VAWT. Observably, the trends recorded in literature give different accounts on how a VAWT behaves in non-uniform wind conditions with no consistent agreement. The aerodynamic characteristics of Darrieus type small scale wind turbine in turbulent environments is an area that does not have much literature. There is need to investigate the behavior of this type of turbines for application in urban environments. Increasing the spread of micro-wind turbines not

only promotes the decentralized generation of energy, but also helps tackle fuel poverty and to achieve reductions in the emission of greenhouse gases (GHGs). Therefore, this study investigated the influence of free-stream turbulence intensity on the aerodynamic performance of a VAWT in a wind tunnel environment.

CHAPTER THREE

METHODOLOGY

3.1 Introduction

This chapter presents the work that was done and the approaches that were used to obtain data. The wind tunnel facility was modified and adjusted to accommodate the rotor and the wedge mechanism. The chapter then discusses the rotor design and dimensions, the wedge turbulence generating mechanism and the measurement assembly for data collection. Finally, the chapter outlines how data was analysed to give the behaviour of the rotor under study.

3.2 Wind Tunnel Facility

The wind tunnel used was an open-circuit suction device with an axial fan located at the outlet. It is set in the Fluid Engineering laboratory, Mechanical Department at the Jomo Kenyatta University of Agriculture and Technology. The tunnel has a total length of 4.6 m with the inlet section measuring 1.2 m by 1.2 m as shown in figure 3.1.

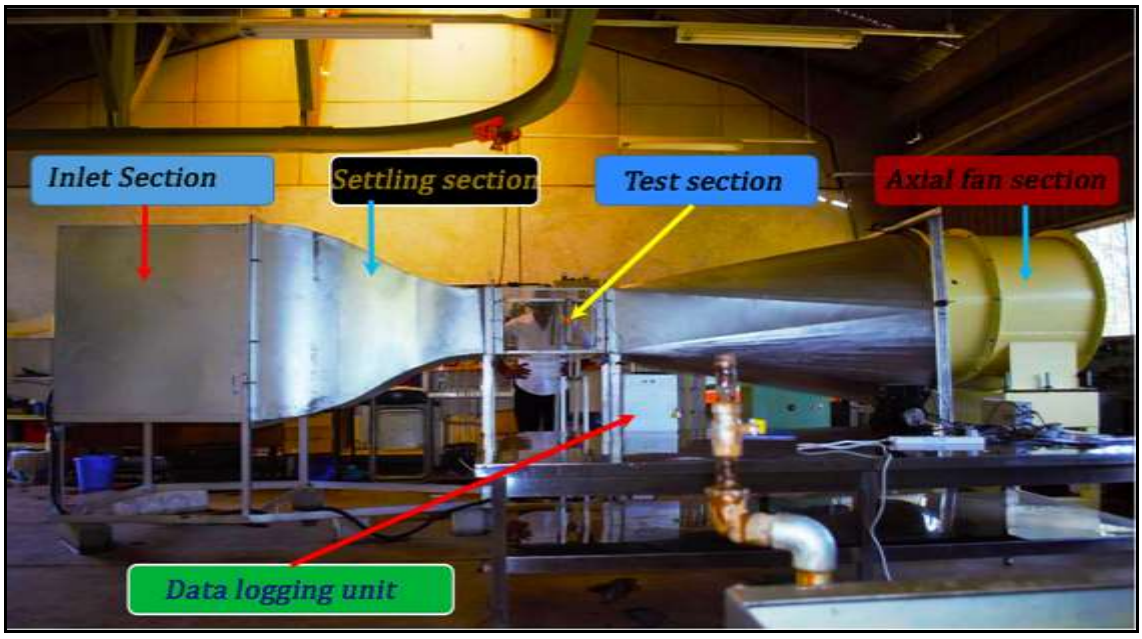

Figure 3.1: Wind Tunnel facility at Mechanical Engineering Department of JKUAT

The tunnel includes a 0.66 m long centralized test section with inlet section 0.44 m by 0.44 m. The inlet is fitted with an array of honeycomb mesh to straighten the wind flow. There is a short settling section after the mesh that allows turbulence and non-uniformities to dissipate then the wind is accelerated by a contraction cone through at a ratio of 7.4:1 into the inlet section of the working section. The working section is fitted with transparent Perspex glass with respective holes created to allow for the insertion of the rotor and measurement instrumentation.

The tunnel suction fan (figure 3.2) was controlled via a variable frequency drive, VFD (figure 3.3) that allowed precise setting of the fan speed in 0.01 Hertz resolution with a maximum speed of about 50 Hz which theoretically would results to tunnel speeds of about 20 m/s. For this experiment the frequency was restricted to about 36 Hz resulting to wind speeds of about 10 m/s; due to structural safety and also to control/reduce the

aerodynamic forces generated on the rotor. Measurements were made with wind speeds ranging from 5 m/s to 10 m/s specifically choosing free-stream velocities of 5 m/s, 7 m/s, 8 m/s, 9 m/s and 10 m/s.

Figure 3.2: Axial suction fan located at the end of the tunnel section

Figure 3.3: Variable frequency drive

3.3 Design of the Wedge turbulence generating mechanism

Levels of free-stream turbulence were generated using active turbulence generating wedge mechanism located at the end of the test section inlet. An active turbulence-generating wedge mechanism was located at the entrance of the test section to generate the required turbulence. This consisted of three elliptical wedges, 0.4 m high, positioned 0.05 m apart across the 0.44 m width inlet section at a distance of 0.5 m away from the rotor which was positioned on the downstream section of the working section as shown in figure 3.4. Tests were first conducted for uniform conditions and then repeated under non-uniform turbulent flow conditions in the presence of a wedge-turbulence generating mechanism then the performance was compared.

Figure 3.4: Turbulence generating wedge mechanism

3.4 VAWT model description

The experiment used a straight-bladed Darrieus VAWT with three blades as in figure 3.5. The three-bladed VAWT rotor was considered as the most appropriate considering research budget cost of manufacturing blade profiles and their mechanical stability. The rotor has a diameter of 0.3 m and height 0.3m thus an aspect ratio, AR=1. The Aspect ratio is the ratio between the blade length and rotor radius. A lower aspect ratio is empirically more desirable since when the aspect ratio falls the Reynolds number rises and this is a desirable condition for better turbine performance. The blades were attached to central shaft of diameter 0.01 m that ran through the top and bottom walls of the test section. The rotor was mounted at the centre but 0.5m downstream along the 0.66 m long test section. Three NACA 0012 symmetrical blades were attached to the central shaft by light aluminium spokes. The symmetric profile was used because it is relatively thick, giving improved performance. Furthermore, the increased thickness gives the blade more resistance to bending and allows easier fixing.

Figure 3.5: The rotor model

In order to create geometrically accurate profiles, the rotor blades were made from high-density form with a smooth fiber glass lining using a 3-D milling machine from Jomo Kenyatta University. This was to give the blades sufficient strength to withstand the centrifugal forces caused by the high rotational speeds. Figure 3.6 shows the rotor model in the test section of the wind tunnel for performance measurements.

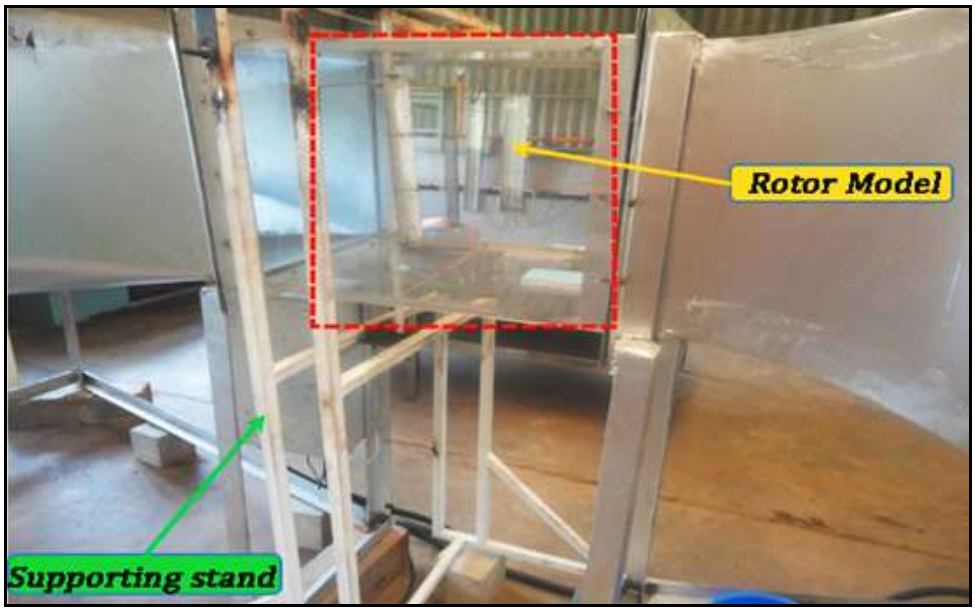

Figure 3.6: The Darrieus VAWT rotor model in a wind tunnel test section

The table 3.1 shows the main features defining the rotor used in the study.

Table 3.1: Main rotor parameters describing the rotor used in the study

Nomenclature	Value	Unit
Turbine type	H-rotor Darrieus type	
Blade profile	NACA 0012 profile	
Number of blades	N = 3	
Chord	c = 0.04	(m)
Solidity	0.8	
Rotor radius	0.15	(m)
Rotor Aspect ratio	AR = 1	

Figure 3.7 gives a schematic illustration of the rotor in the presence of wind and the data acquisition system.

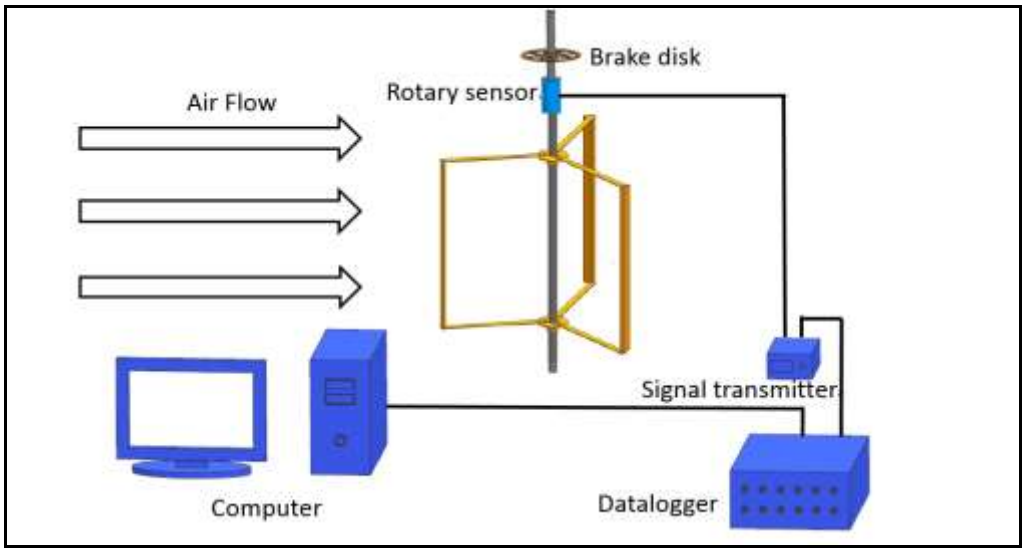

Figure 3.7: Schematic illustration of the Darrieus VAWT type experimental apparatus

3.5 Instrumentation and data acquisition system for the VAWT

3.5.1 Wind velocity measurement

The free-stream reference wind velocity in the working section was be measured using a Pitot-static pressure probe. Figure 3.8 is a representation of a Pitot-static pressure tube. A mechanical ball bearing disc brake was developed and employed in maintaining reasonably constant average rpm by varying the load applied to the small wind turbine. Thus the behavior of the power coefficient, CP, was observed at different rpm.

The free stream reference wind velocity was measured and set using a Pitot-static pressure tube at the beginning of each test. The Pitot-tube was positioned at different heights spanning the test section to determine the wind profile. The Pitot-tube records the difference in static and total pressure through a differential-pressure transducer that operates by application of Bernoulli's equation.

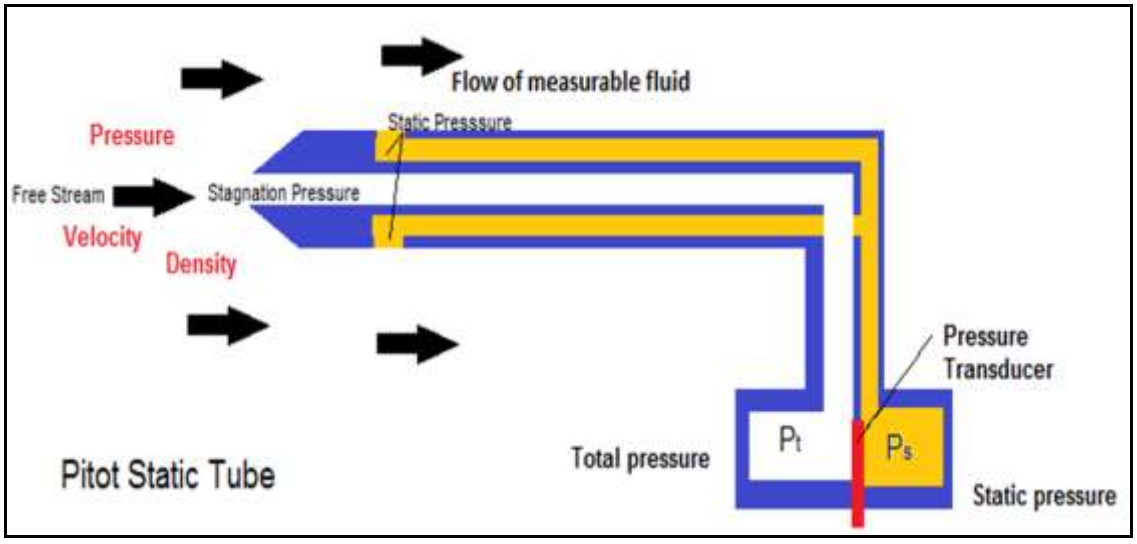

Figure 3.8: Pitot static pressure tube

The Pitot tube is used as a speedometer. A central hole is drilled down the axis of the tube and pointed in the direction of the flow while side holes are positioned perpendicular to the flow. The side holes were then connected to one side of a pressure differential transducer while the central hole was connected to the other side. The difference in the pressures was measured by the transducer which uses an electronic strain gauge to measure the strain in a thin element.

The outside holes being perpendicular to the flow, experience the effect of pressure from the random component of the air velocity, called the static pressure. The central hole however was pressurized by both the random element velocity and the incoming flowing velocity element, which make up the total pressure as is suggested by Bernoulli's equation. The transducer finds the difference in these two pressures, dynamic pressure. Velocity is computed from the Bernoulli's equation as:

$$Static\,\mathrm{Pr}essure + dynamic\mathrm{Pr}essure = Total\,\mathrm{Pr}essure \quad \ldots\ldots\ldots\ldots\ldots\ldots\ldots\ldots 3.1$$

$$P_s + \rho \times \frac{v^2}{2} = P_t \quad \ldots\ldots\ldots\ldots\ldots\ldots\ldots\ldots\ldots\ldots\ldots\ldots\ldots\ldots\ldots\ldots\ldots\ldots\ldots\ldots 3.2$$

hence velocity is presented as (Manwell *et al*., 2009);

$$V^2 = \frac{2(P_t - P_s)}{\rho} \quad \text{.....3.3}$$

The output signal from the transducer was connected to a National Instruments Data Acquisition Card (NI USB-6008, 8 inputs, 12kS/s, multifunction I/O) then through a USB cable to a Laboratory Virtual Instrument Engineering Workbench (LabVIEW) program coded on the computer. The LabVIEW program is coded to allow the velocity to be read after different time intervals as desired. The data was logged and saved for analysis.

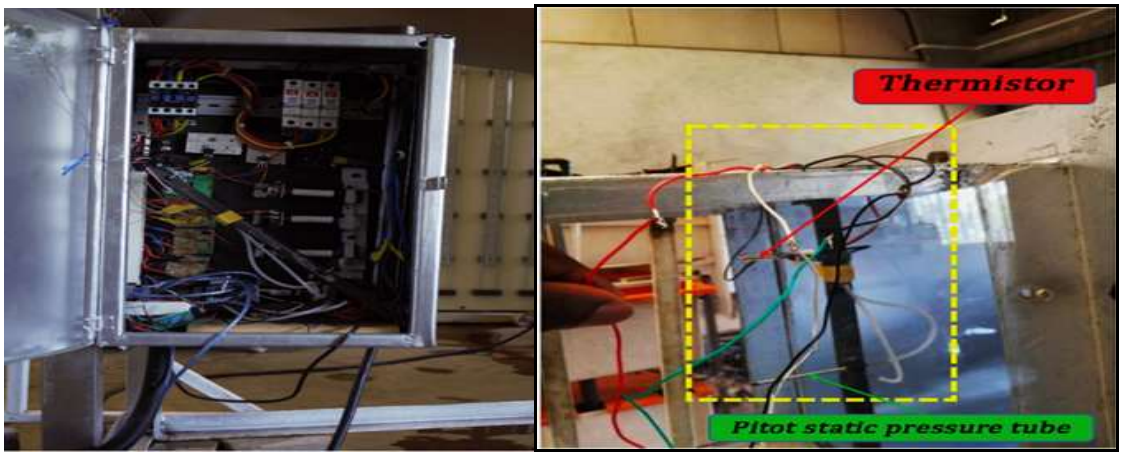

Figure 3.9: Pitot-pressure tube and thermistor measurement assembly

3.5.2 Torque and Power Measurements

Torque was measured directly using a torque detector model SS-500 with a torque range 0 Nm to 50 Nm and the value indicated on a torque meter model ONO SOKKI TS-2800. The rotor shaft was coupled directly to the torque detector which was then connected to the torque meter. Rotational velocity was also obtained from the

transducer which is fitted with MP-981 magnetic detector with maximum rotational velocity of 6000rpm. The setup is as shown in the Figure 3.10.

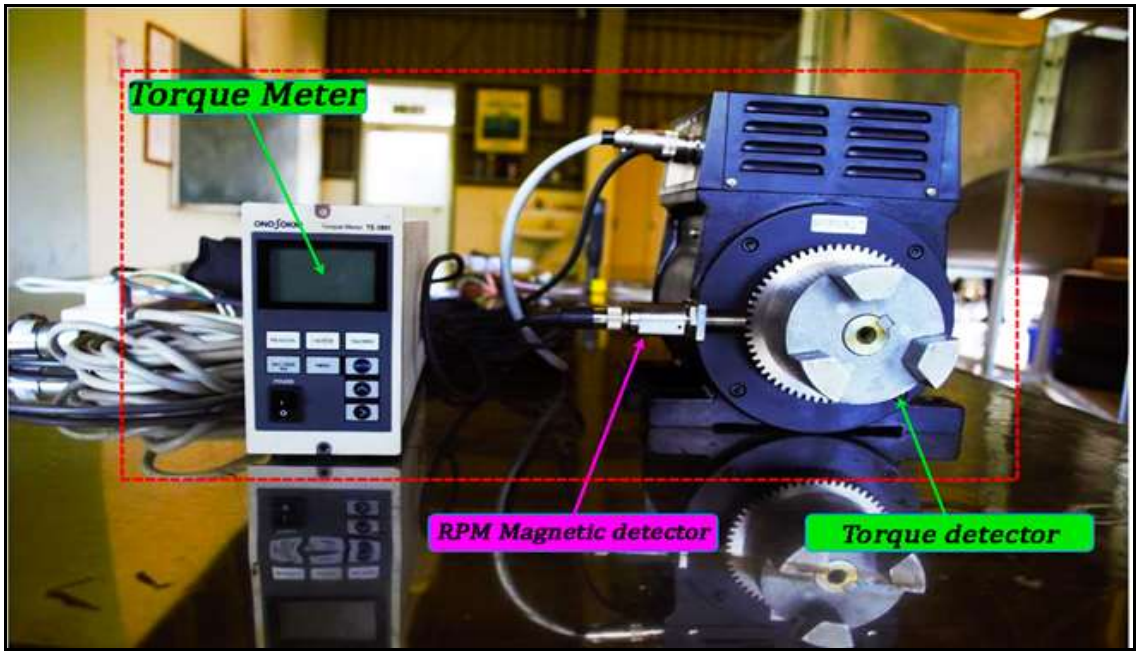

Figure 3.10: Torque meter, RPM detector and the drive side of the torque detector

To quantify the aerodynamic performance of the wind turbines, dimensionless performance parameters torque coefficient Cm and power coefficient CP are expressed as functions of tip speed ratio, λ as defined by equation 2.9, equation 2.10 and equation 2.11 respectively.

Power coefficient, CP is the actual power produced by the wind turbine expressed as a ratio of the actual wind power flowing into the rotor at a given wind speed. This was used to measure the overall efficiency of the rotor. The power coefficient was tabulated for different wind speeds so that the study could estimate the electric power output. Power extractable from the wind was calculated using equation 2.8.

The wind rotor was not able to self-start in some configurations like is the case with most VAWTs since enough torque is not generated to start the rotor thus a starting

mechanism was employed. An electrical motor and electrical clutch were used with the clutch disengaging immediately a desired rotational velocity was achieved. It is effectively observed that the self-starting ability was improved in the case of turbulent non-uniform wind such that the rotor did not need as much help as in the case of uniform flow. This is consistent with studies made by (Edwards, 2012; Danao *et al*., 2012).

3.6 Data processing and analysis

The Pitot-static pressure probe was positioned at different heights within the wind tunnel test section and wind velocity measured at time interval of 10 seconds in the absence of the rotor model. This data was used to determine the wind velocity and turbulence intensity profiles. Due to high costs and time constraints, mathematical models were employed to determine vertical wind shear for this study. Power law (equation 2.2) was preferred over log-law (equation 2.1) because of its simplicity and since it seems to give a better fit to most of the data over greater height range and higher wind conditions (Wekesa *et al*., 2016; Mikkelsen, 2013). A Pitot-static pressure probe was placed in the middle of an empty tunnel test section to determine the reference wind speed. Three more measuring positions were spanned by the probe below and above the reference level.

Wind speeds were recorded using LabVIEW software programmed to record the speeds of wind after every 10 seconds for a minimum period of 5 minutes in each test. This was done for both uniform and non-uniform conditions in the presence of the turbulence mechanism. Graphs were created and smoothened using SigmaPlot14 and in each case they show the behaviour of wind speeds under uniform conditions and how that fluctuates under non-uniform conditions for different heights.

Power performance parameters discussed were obtained using mathematical expressions and the data obtained. The same data was expressed in form of graphs developed by the statistical package SigmaPlot14.

CHAPTER FOUR

RESULTS AND DISCUSSION

4.1 Introduction

This chapter aims to present the results for wind velocities and describe how power performance characteristics of the turbines were compared for uniform and turbulent non-uniform conditions. Graphs indicating the variation of wind with time are presented and discussed to show how the generated turbulence causes fluctuation in wind speeds about the mean. This is compared to the uniform wind conditions measured in the absence of the wedge mechanism. Power performance of the turbines in the tested conditions is presented as a relationship between power and torque coefficient with tip speed ratio.

4.2 Wind velocity and Turbulence Intensity Profiles

Using the data obtained for wind velocity, graphs for wind velocity (Figure 4.1) and turbulence intensity profiles (Figure 4.2) were generated using SigmaPlot14.

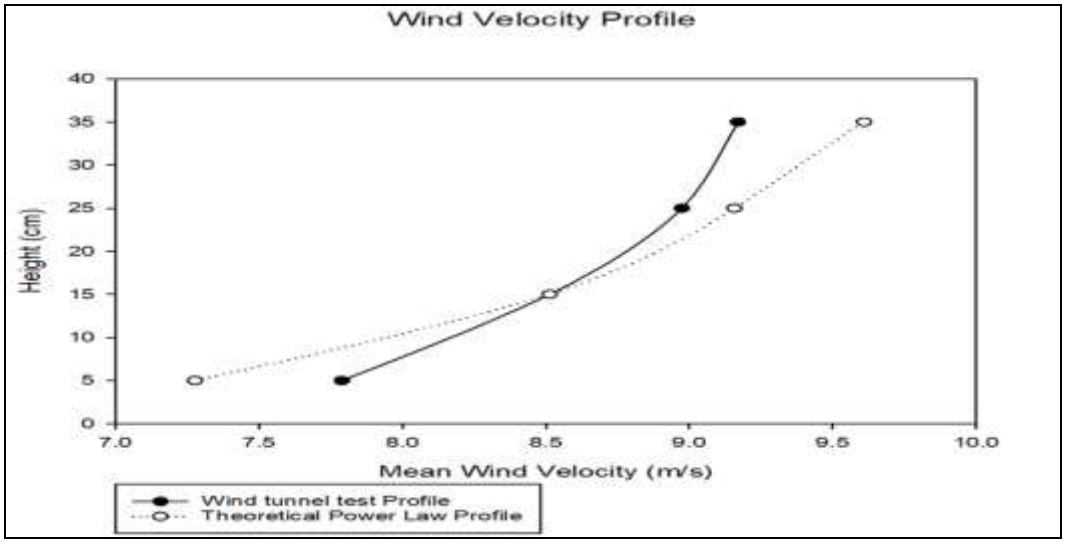

Figure4.1: Mean wind velocity profile

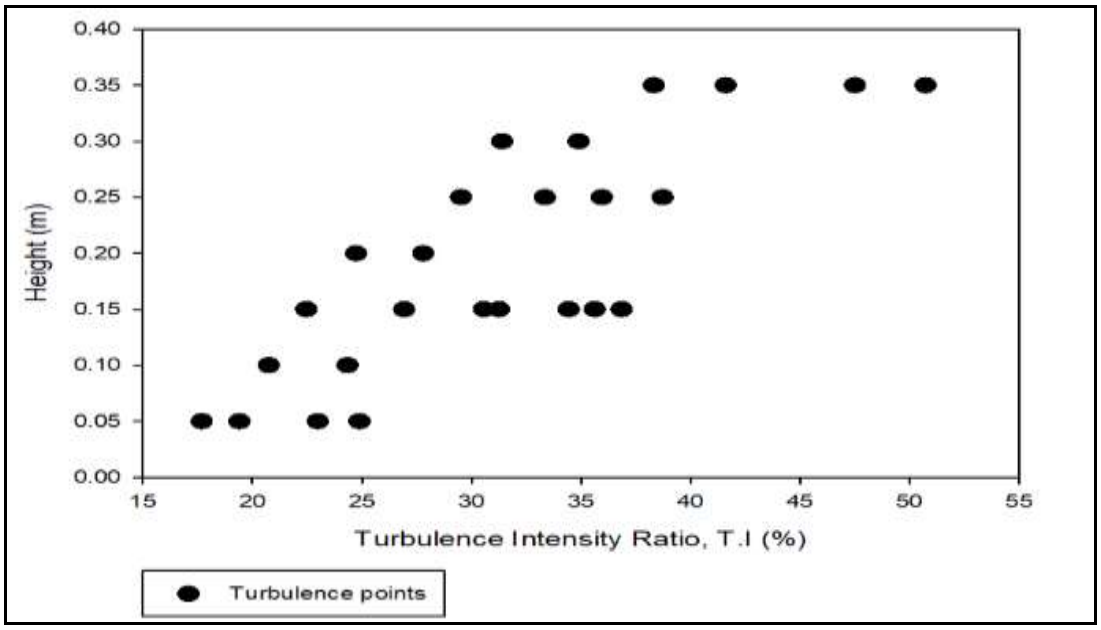

Figure 4.2: Turbulence intensity profile

Figure 4.1 and Figure 4.2 show the mean wind velocity profile and the turbulence profile respectively for this study. The wind velocity profile shows the relationship between wind speeds at one height and those at another. In this study, the wind velocity profile was indeed a match with the desired urban area of study with a theoretical power law index of 0.1429 (Wekesa *et al*., 2017). Temperature measurements done within the test section show that there is no variation in temperature with height within this section. The variation in wind shear with height is attributed to the surface friction occurring between the wind and the surface in this case the Perspex enclosing the test section; and also the high density of air at low surfaces which require more wind kinetic energy to move as compared to less dense wind in the middle. Turbulence intensity is shown to be fluctuating between 17.69% and 50.74%. Studies done by Lubitz (2014) used turbulence intensity between 14% and 18% which was classified as either high or low. Mojtaba *et al*., (2015) observed the behaviour of turbines under three levels of intensity: 5%, 7.5% and 15%. This study does not limit the scope of turbulence intensity. According to (Wagner and Mathur, 2012), turbulence in wind can scale up to 150% about the mean wind speed. Secondly, this study's main objective is to relate the performance for uniform and non-uniform conditions.

4.3 Uniform and non-uniform wind characteristics

Figure 4.3 to Figure 4.10 show selected graphs of wind speeds against time at various heights within the wind tunnel. It was observed that at lower heights of 5 cm from the surface of the test section, uniform wind consistently had higher and more stable wind speeds. The design of the wedges in this study are elliptic with a wide bottom and narrows as they increase in height. This design was chosen to represent urban environments that usually have buildings, vegetation and other infrastructure concentrated at the lower heights and the crowding reduces with height. The lower speeds in turbulent conditions are attributable to blockage by the wider surfaced wedges, high density of air at the bottom that requires more kinetic power to flow and surface friction with the surface of the test section. When the height is increased, the wind under turbulent conditions is seen to fluctuate about the mean wind speed from

uniform condition with quick jumps from very low wind speeds to very high wind speeds within a very short time. In Figure 4.3 where the height is 35 cm and VFD set at 26 Hz, the wind speed jumps from 2 m/s at the 90 seconds mark to 7 m/s at 100 seconds mark. Figure 4.4 at height 35 cm VFD frequency 28 Hz the wind speeds in turbulent conditions shifts from 2.3 m/s at 180 seconds to 11.5 m/s at 190 seconds. This is a representation of the behaviour of wind in normal fluctuating urban environments where wind shifts and changes within very short time periods. Surface roughness is represented by the wedges.

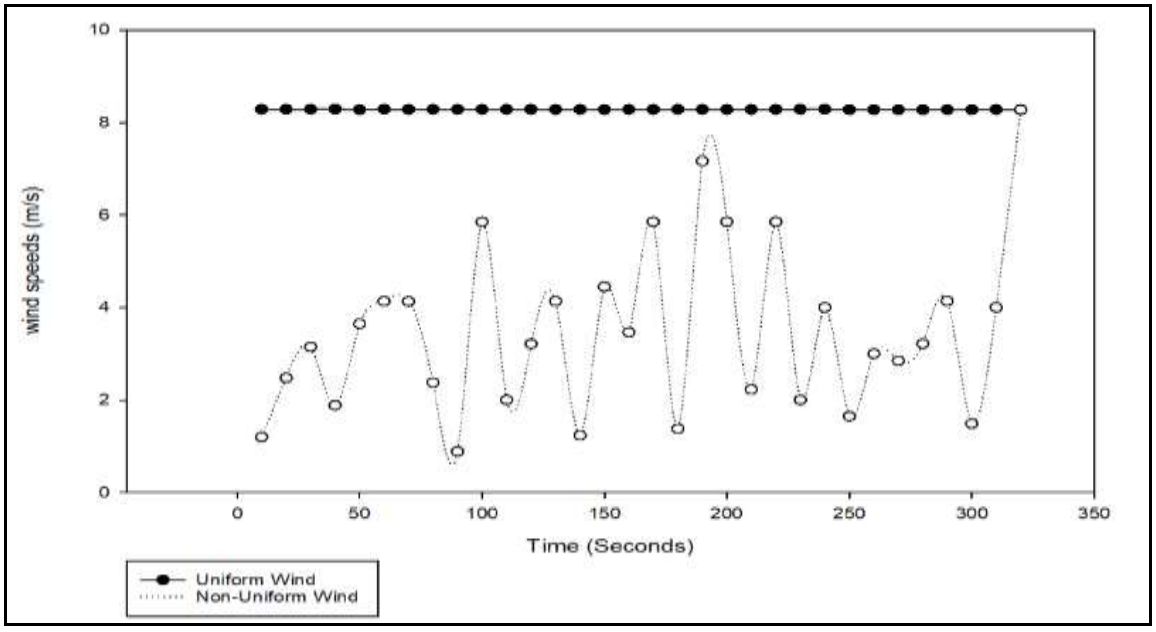

Figure 4.3: Uniform and non-uniform wind at height 5 cm, VFD 28Hz

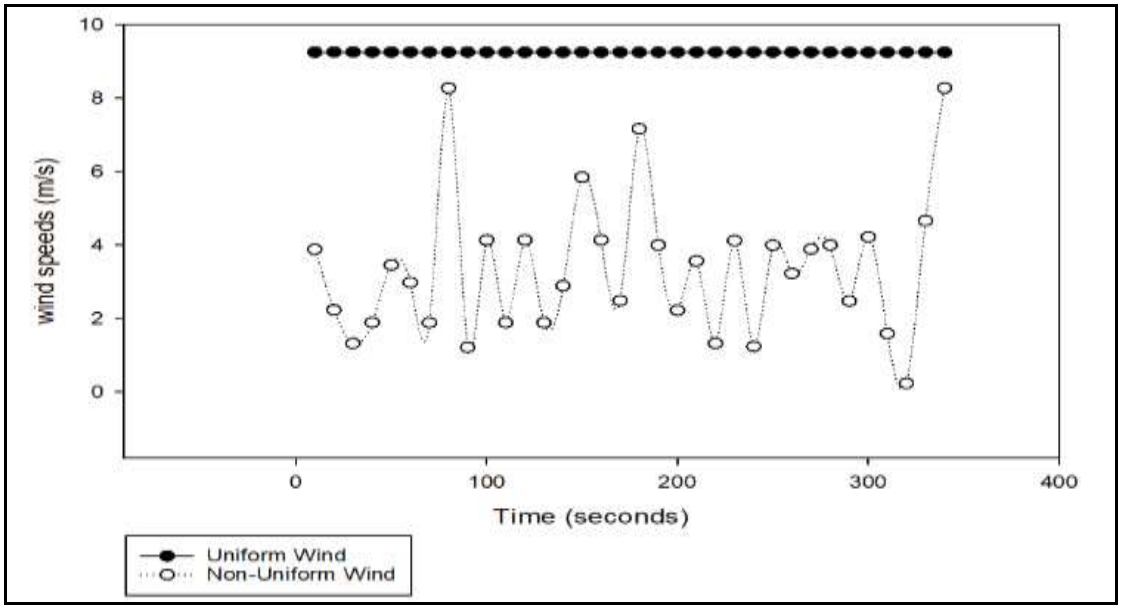

Figure 4.4: Uniform and non-uniform wind at height 5 cm, VFD 30 Hz

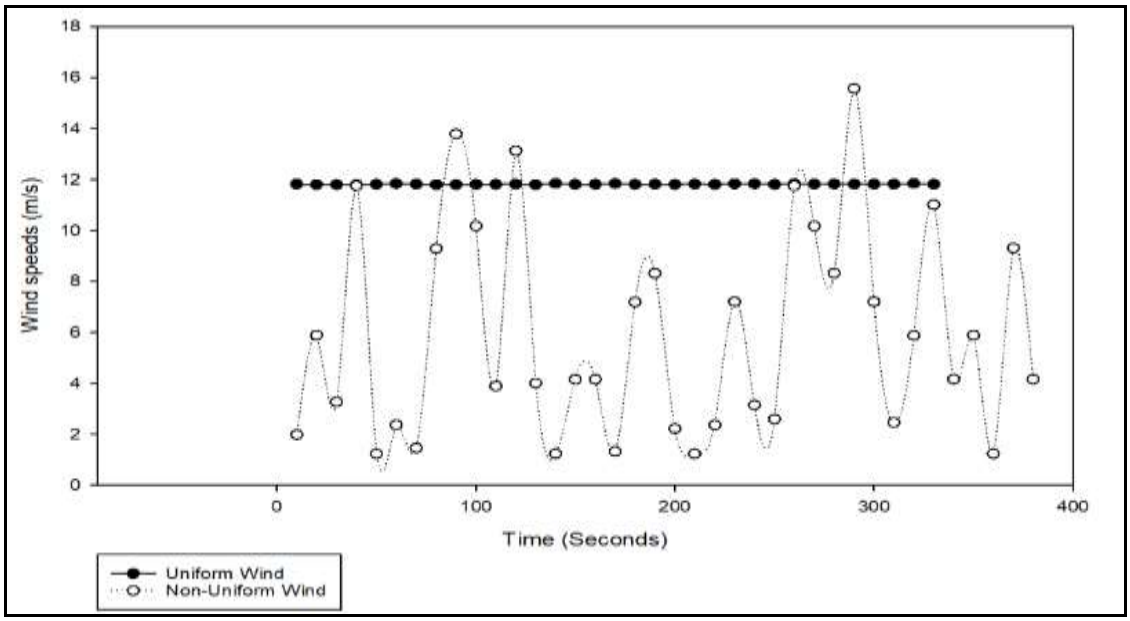

Figure 4.5: Uniform and non-uniform wind at height 15 cm, VFD 34 Hz

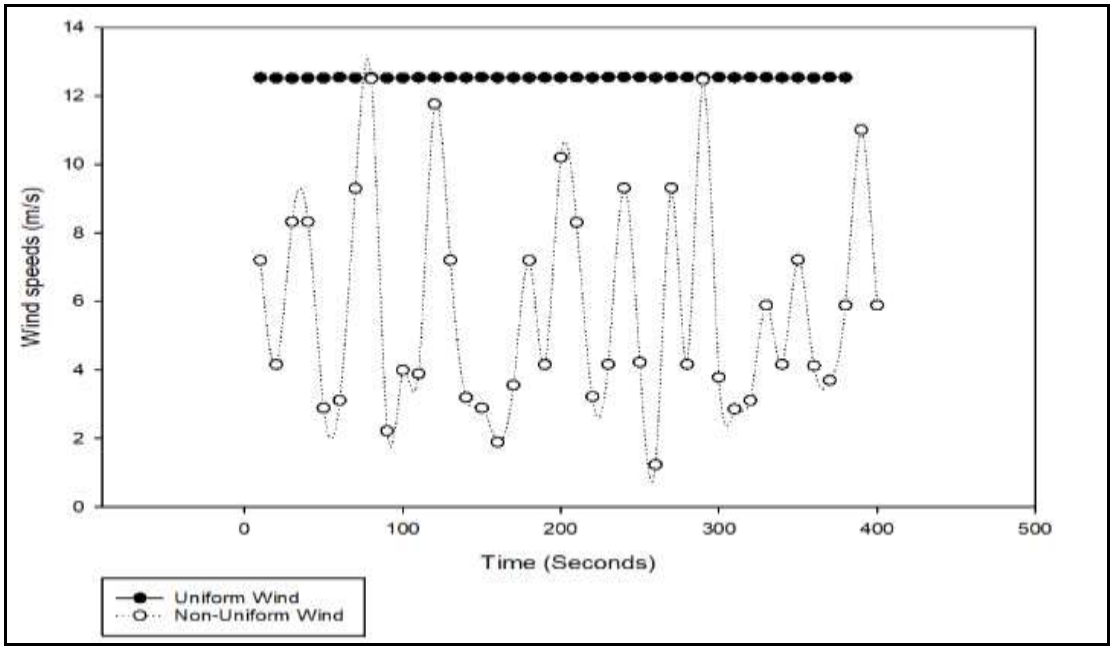

Figure 4.6: Uniform and non-uniform wind at height 15 cm, VFD 36 Hz

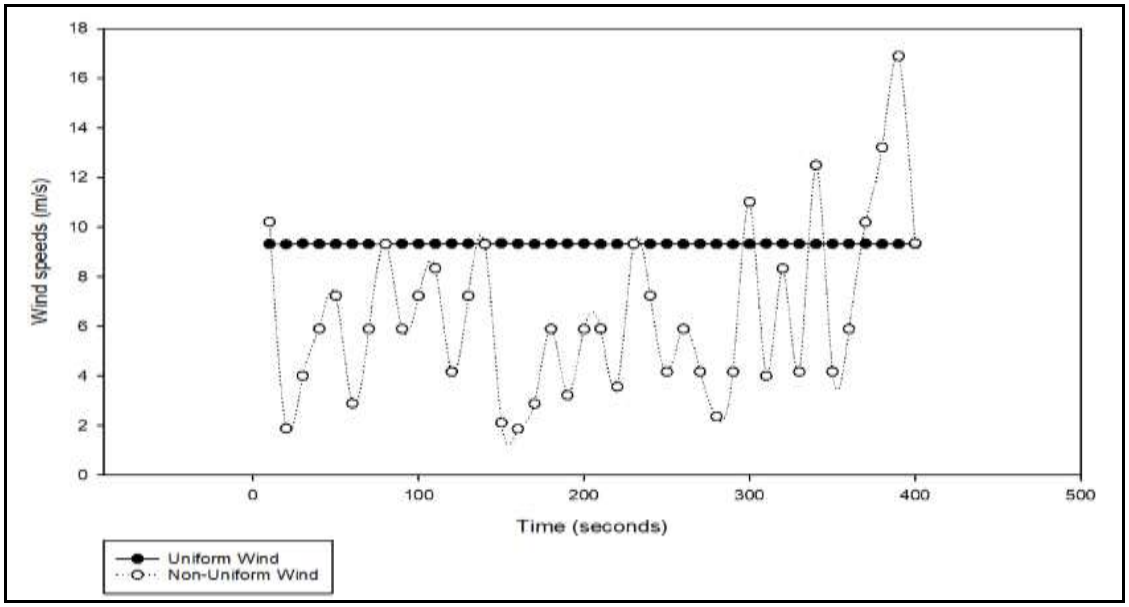

Figure 4.7: Uniform and non-uniform wind at height 25 cm, VFD 30 Hz

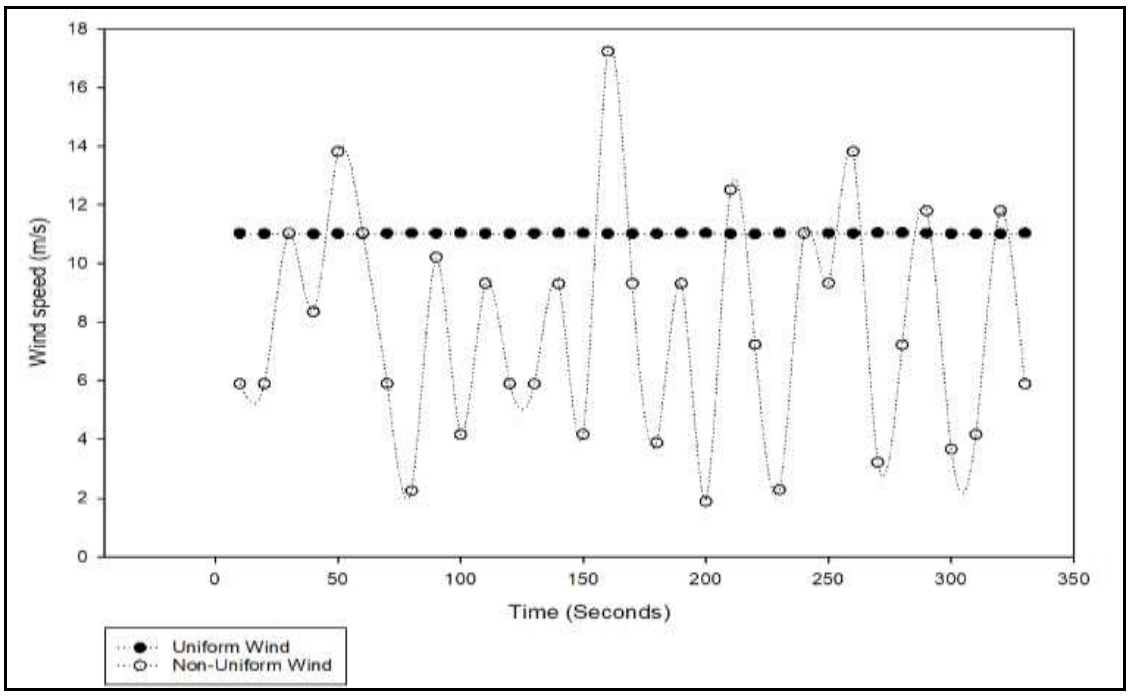

Figure 4.8: Uniform and non-uniform wind at height 25 cm, VFD 34 Hz

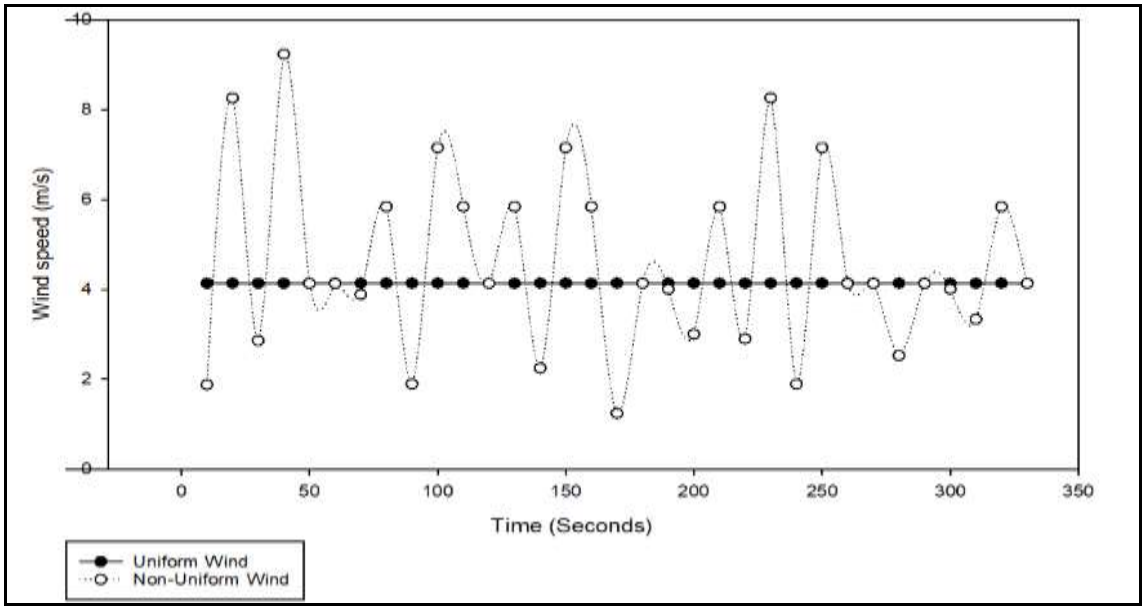

Figure 4.9: Uniform and non-uniform wind at height 35 cm, VFD 26 Hz

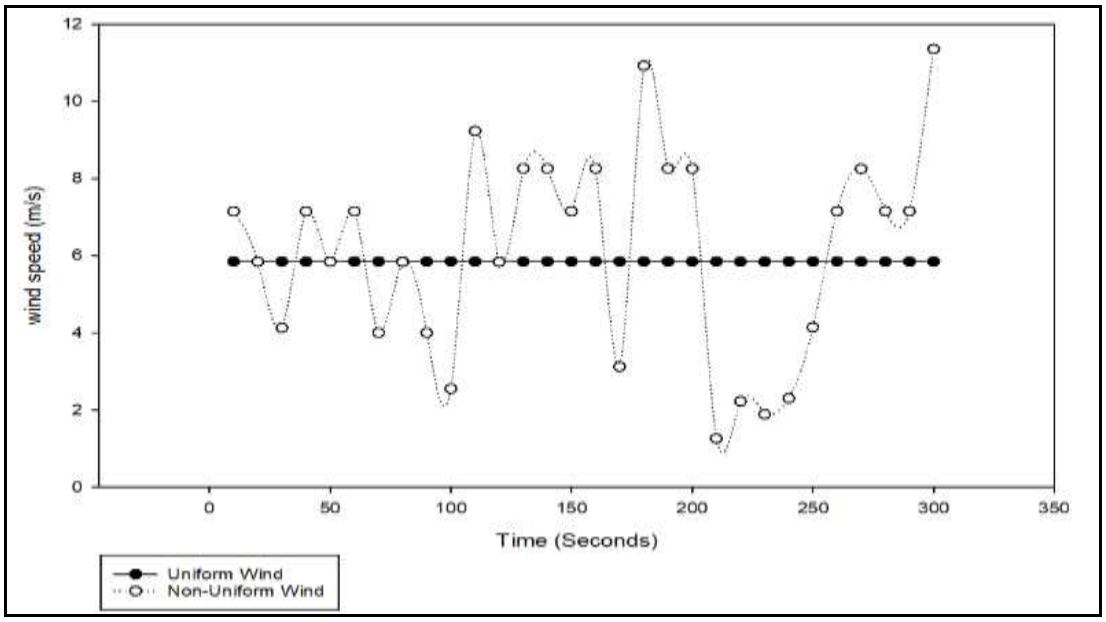

Figure 4.10: Uniform and non-uniform wind at height 35 cm, VFD 28 Hz

4.4 Power performance measurements

Analysis is made for the performance of VAWTs in both uniform and non-uniform conditions and the two results compared to investigate the aerodynamic performance of the turbine. Following published work in (Pagnini *et al*., 2015, Wekesa *et al*., 2016, Mojtaba *et al*., 2015, Lubitz. 2014) as well as results from this study, it was observed that the Darrieus VAWT model was not able to self-start even under considerably high wind speeds. A start up mechanism consisting of an electronic motor and clutch was used to start the turbine accounting for the negative CP band at lower tip speed ratio (λ).

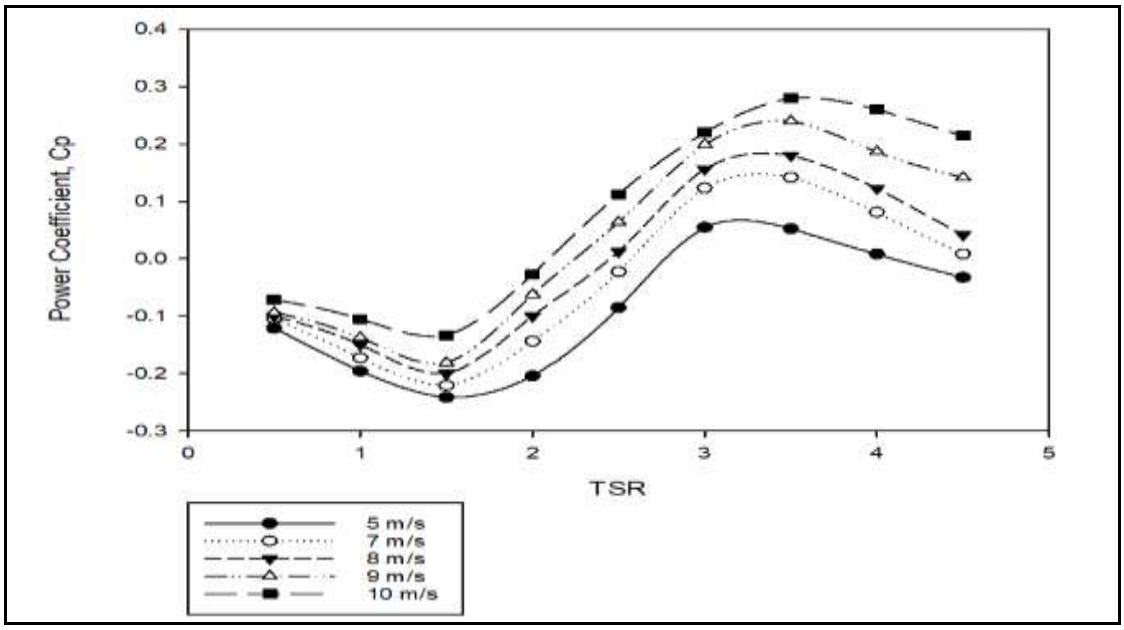

Figure 4.11: CP distribution as a function of TSR under uniform conditions.

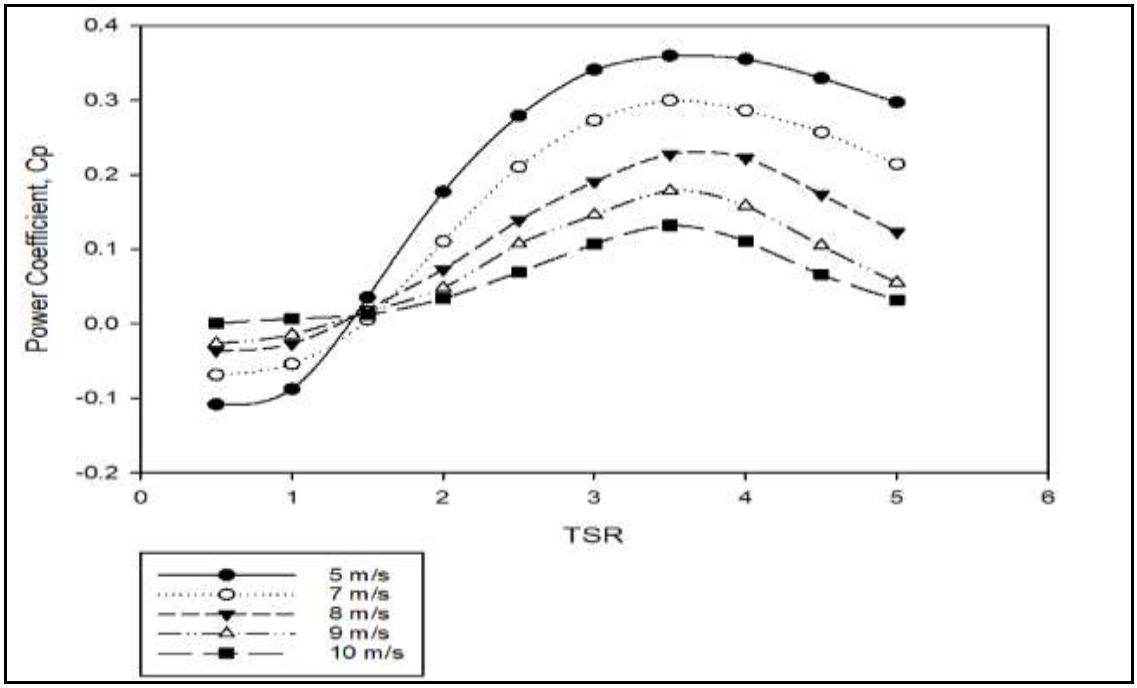

Figure 4.12: CP distribution as a function of TSR for non-uniform turbulent flow

Power coefficient and torque coefficient are expressed as functions of tip speed ratio from Figure 4.11 to figure 4.14. Figure 4.11 shows that for the uniform flow, CP distribution power curve continues to shift upwards with increasing free stream velocity throughout the range of TSR under study. The power curve shifts up to an optimum CP = 0.2822 at uniform wind speeds of 10 m/s. Figure 4.12 on the other hand shows fluctuations on the curve with both increase and decrease in power performance recorded at low and high wind speeds respectively. Under turbulent non-uniform conditions, the optimum power is observed at CP = 0.36 at flow wind speeds of 5 m/s. In both cases, the maximum CP range is obtained at λ ranging between 3.5 and 4. Turbulence can be associated with delaying of dynamic stalling at lower angles of attack. The interaction of turbulent air particles with the surface boundary layer delays flow separation on the aerofoil until a higher angle of attack. This postpones flow separation over the blade surface.

The power curves for both uniform and non-uniform flow reveal the inability of the rotor to self-start. The power curves plummets to a negative CP band area when the rotor starts up from rest and keeps increasing through the λ range. This is consistent with studies by Danao *et al*., (Danao *et al*., 2014) and Kirke. An electronic motor and clutch powers the rotor in this band and the power, in return, is spent to get the rotor to a steady sustainable speed. This region is called a dead band. It is, however, observed in the non-uniform flow that at high wind speeds, the rotor is capable of self-starting. At 10 m/s the rotor was able to self-start. High wind speeds and the turbulence effects are able to overcome the resistive torque present.

While the power from the turbine increases with increasing wind speeds for uniform flow, there is generally more power produced at lower wind speeds for non-uniform flow. The value of the power coefficient is generally lower for uniform flow as compared to non-uniform flow indicating that for the experimental rotor under investigation, turbulence increased the power production. Non-uniform turbulent conditions resulted to more power generated at low wind speeds and reduced self-

starting speeds. The turbine attains stable speeds between TSR values ranging from 1.5 to 2 for non-uniform turbulent flow and from 2 to 2.5 for uniform flow.

Power coefficient distribution increased drastically for low wind speeds of 5 m/s and 7 m/s in the non-uniform flow. Despite the general trend of increasing CP distribution in the non-uniform flow, it is revealed that at 8 m/s the rise is not as drastic as it was in the previous cases. As the wind speeds increase to 9 m/s and 10 m/s the CP distribution keeps shifting downwards. This reduction in power coefficient at high wind speeds in the non-uniform conditions shows that the turbine experiences furling at some point. The experimental rotor design starts experiencing furling at wind speeds of about 8 m/s. Despite the rotor moving at very high speeds, detrimental effects are observed that reduce the power generation of the wind turbine.

Further analysis was done for torque coefficient distribution. There is a notable increase in the torque coefficient in the presence of turbulence at lower wind speeds as compared to the uniform flow. The torque coefficients takes maximum peaks of 0.0182, 0.0410 and 0.0522 at wind velocities of 5 m/s, 7 m/s and 8 m/s respectively for uniform flow, figure 4.13.

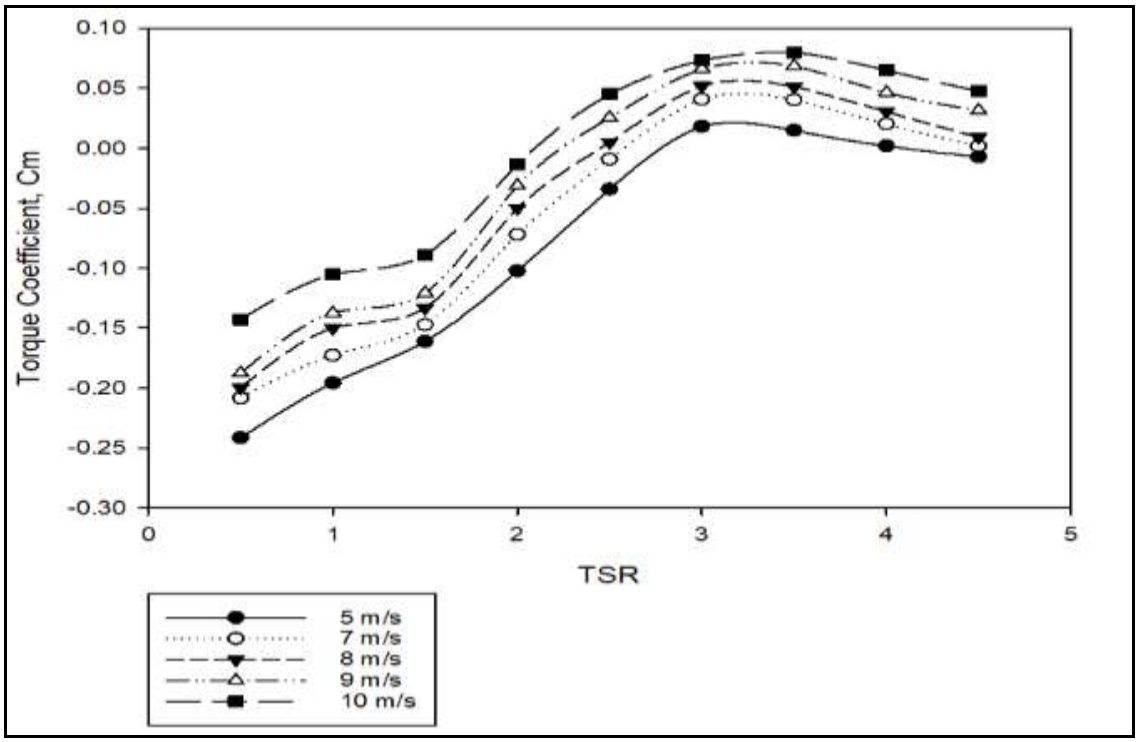

Figure 4.13: Torque coefficient vs TSR for various wind speeds in uniform flow

Noticeably, for non-uniform turbulent flow, the value for torque coefficient increases to peak at 0.1137, 0.0911 and 0.651 at wind speeds of 5 m/s, 7 m/s and 8 m/s respectively (Figure 4.14).

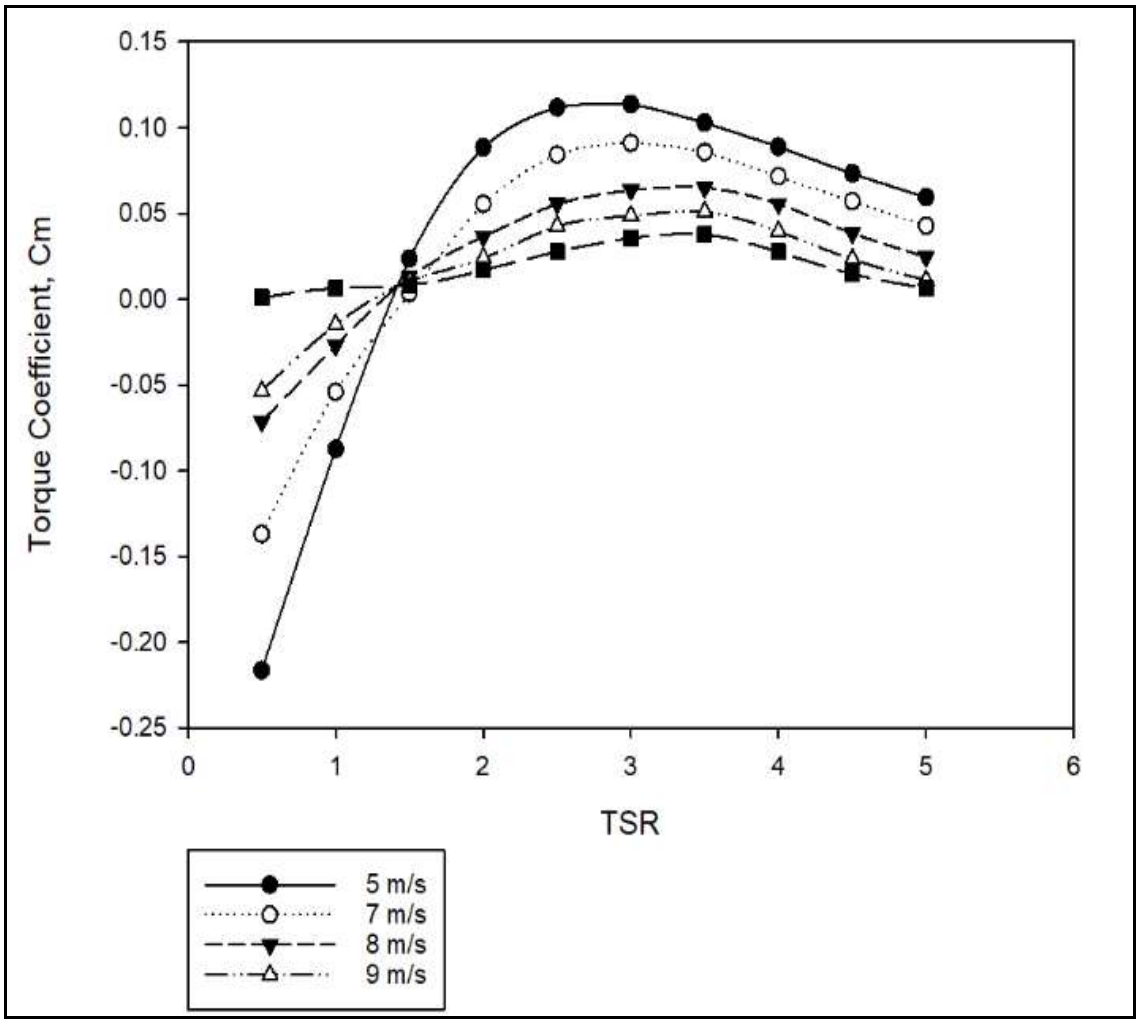

Figure 4.14: Torque coefficient vs TSR for various wind speeds in non-uniform flow

However, torque coefficient reveals a substantial decrease at higher wind speeds in the case of non-uniform flow. The torque coefficient drops from 0.0686 and 0.0800 at 9 m/s and 10 m/s respectively for uniform flow to 0.0510 and 0.0357 for 9 m/s and 10 m/s respectively for non-uniform flow.

The torque coefficient distribution curve reveals that the uniform inflow has reduced power coefficient as compared to the non-uniform turbulent flow at wind speeds of 5 m/s, 7 m/s and 8 m/s. However, for wind speeds 9 m/s and 10 m/s there is reduced

torque coefficient in the non-uniform flow as compared to the uniform flow. This ideally reveals that this is the operating range for the turbine above the cut-in speed and below the turbines cut-out speed referred to as the furling. At 9 m/s and 10 m/s there is reduced power production for non-uniform conditions, a clear suggestion that furling will be reached faster in non-uniform flow than in the uniform flow. The rotor tested would operate best in the range 5 m/s to 8 m/s.

Maximum CP and Cm are plotted as functions of wind speeds to further explain the trends for uniform and non-uniform flow as in Figure 4.15 and figure 4.16. Power and torque coefficient increase with increasing wind speeds for uniform flow while the highest values for non-uniform flow are observed at the lower wind speeds. The turbine is seen to operate at its maximum for non-uniform flow in the range of 5 m/s to 8 m/s. Beyond these velocities both power coefficient and torque coefficient reduce drastically. This is because the turbine has approached furling speeds and the gusty wind within this regime cause furling and reduced energy production. It is also revealed that at wind speeds of 5 m/s to 8 m/s there is more power harnessed in turbulent conditions as compared to uniform flow. However, at 9 m/s and 10 m/s more power is produced by the uniform flow. This means that in a uniform flow, the turbine delays before reaching furling speeds.

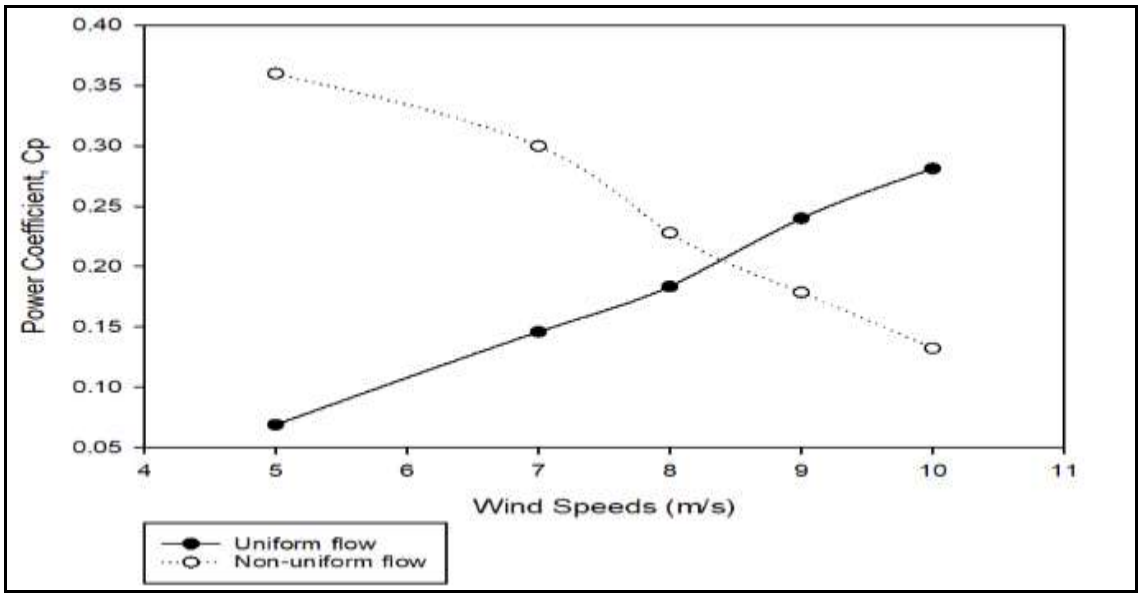

Figure 4.15: Power coefficient as a function of wind speed for uniform and non-uniform flow.

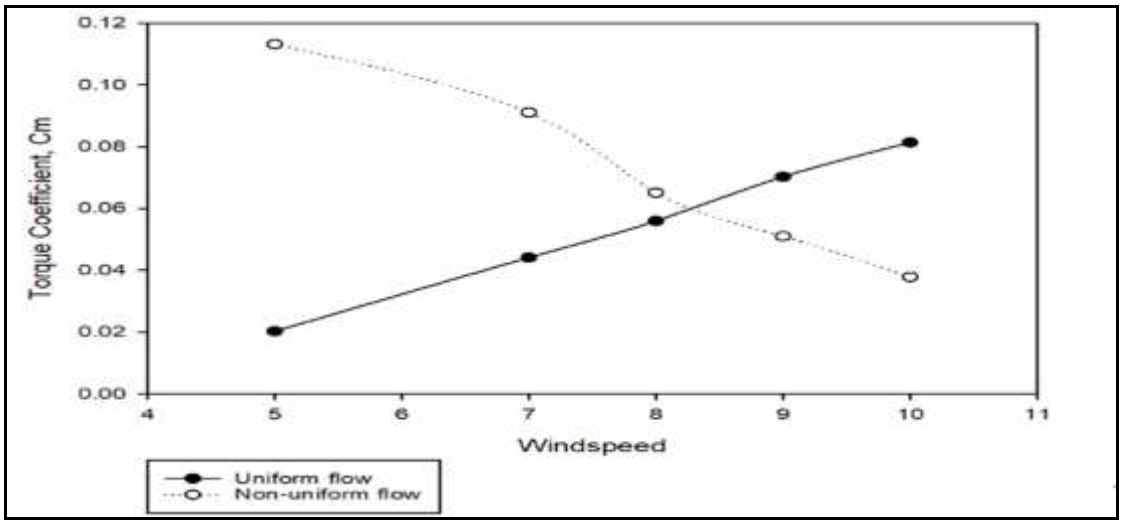

Figure 4.16: Torque coefficient as a function of wind speed for uniform and non-uniform flow

CHAPTER FIVE

CONCLUSIONS AND RECOMMENDATIONS

5.1 Conclusions

The research involved development of a mechanism to generate a non-uniform turbulent inflow within a wind a tunnel. This included development of a Darrieus-type VAWT rotor within the laboratory to measure the VAWT rotor wind performance for both uniform and non-uniform turbulent wind conditions. Performance parameters were then compared to characterize the effect of turbulence on the rotor.

1) Performance of the turbine in uniform conditions increases with increasing wind speeds with the lowest power produced at the lower wind speeds and the highest power at the higher wind speeds below cut-out speed. Non-uniform turbulent conditions however, show maximum power performance at the lower wind speeds above cut-in and power production reduces as the wind approaches cut-out speeds.
2) Non-uniform wind resulted into improved self-starting ability by reducing the self-starting speed of the rotor. The rotor is able to start at lower TSR as compared to the case in uniform conditions. This was attributable to the rapid decay in the lower moment when the rotor starts rotating as a result of reduction of the relative velocity between free-stream wind and the VAWT rotor. It was also observed that at high free-stream speeds, of 10 m/s in this study, the rotor was able to self-start under non-uniform conditions.
3) Uniform flow has more power production at higher speeds compared to non-uniform conditions. This indicates that there is delay before reaching cut-out speeds for uniform conditions since they produced more power above 9 m/s while in non-uniform conditions this speed marked the beginning of furling. Self-starting is improved but power production for this rotor reduces. As a

result, the VAWT rotor under study would operate best at rated wind speeds ranging from 5 m/s to 8 m/s.

5.2 Recommendations

The results from the study is important to wind energy technology stakeholders and industrial aerodynamics applications that require designs for wind turbines reflecting urban turbulent environment. Although the methodology developed in this study including similar effects observed in the wind tunnel can be transferable to full-scale VAWT rotors, the results may suffer from scaling effects. This is due to the fact that atmospheric turbulence is different from wind tunnel generated turbulence. Therefore, we recommend that in future, experimental investigations should look into scaling effects in wind tunnels in order to compare the results from those of large scale wind turbines. Further, Particle Image Velocimetry (PIV) techniques may be used to characterize the behaviour of air around the rotor.

REFERENCES

Baker, J. R., (1983). Features to aid or enable self-starting of fixed pitch low solidity vertical axis wind turbines. *Journal of Wind Engineering and Industrial Aerodynamics, 15*(1–3), 369-380.

Bertenyi T, Wickins C, & McIntosh S., (2010). Enhanced energy capture through gust tracking in the urban wind environment. *48th AIAA Aerospace Sciences Meeting Including the New Horizons Forum and Aerospace Exposition*: *48,* 1–7

Chong W. T., Fazlizan A., Poh S. C., Pan K. C., Hew W. P., & Hsiao F. B. (2013). The design, simulation and testing of an urban vertical axis wind turbine with the Omni-direction-guide-vane. *Applied Energy*. *2*(5), 145-159.

Danao, L. A., Qin, N., & Howell, R., (2012). A Numerical study of blade thickness and camber effects on vertical axis wind turbines. Proceedings of the Institution of Mechanical Engineers, Part A: *Journal of Power and Energy*, *2*(3), 146-155.

Gagliano, A., Francesco, N., Francesco, P., & Alfonso, C., (2013). Assessment of micro-wind turbines performance in the urban environments: an aided methodology through geographical information systems. *International Journal of Energy and Environmental Engineering*. *4,* 43

Healy, J. V., (1978). The Influence of blade camber on the output of vertical-Axis wind turbines. *Wind Engineering, 2*(3), 146-155.

Healy, J. V., (1978). The Influence of blade thickness on the output of vertical axis wind turbines. *Wind Engineering*, *2*(1), 1-9.

Jacobs, E., &Sherman, A., (1937) Airfoil section characteristics as affected by variations of the Reynolds number. *Technical Report No. 586, National Advisory Committee for Aeronautics,* Washington, D.C.

John, W. T. & Anthony, D. W., (2006). *Renewable Energy Resources*. London: Taylor and Francis Group.

Kaldellis, J. K, & Zafirakis, D. (2011). The wind energy revolution: a short review of a long history. *Renewable Energy*. *36*, 1887–901.

Kirke, B. K., (1998). *Evaluation of Self-starting Vertical Axis Wind Turbines for Stand-Alone Applications*. Unpublished Ph.D. thesis, Gold Coast Australia: Griffith University,

Kooiman S. J., Tullis S. W., (2012) Response of a vertical wind turbine to time varying wind conditions found within the urban environment. *Wind Engineering. 34*(4), 389-401.

Lubitz, W. D., (2014). Impact of ambient turbulence on performance of small wind turbine. *Renewable Energy*. *61*, 69-73.

Manwell, J.F., McGowan, J.G. & Rogers, A.L., (2009). *Wind Energy Explained Theory: Design and Application*. West Sussex, United Kingdom: John Wiley & sons Ltd.

McIntosh S., (2009). *Wind Energy for the Built Environment.* Cambridge: University of Cambridge.

McIntosh, S., Babinsky, H., & Bertenyi, T., (2007). Optimizing the energy output of vertical axis wind turbines for fluctuating wind conditions, in: *45th AIAA Aerospace Sciences meeting and exhibit*, Reno, Nevada

McIntosh, S., Babinsky, H., & Bertenyi, T., (2008). Unsteady power output of vertical axis wind turbines operating within a fluctuating free-stream, in: *46th AIAA Aerospace Sciences meeting and exhibit*, Reno, Nevada

Mojtaba, A. B., Carriveau, R., & Ting, D. S. K., (2015). Performance of vertical axis wind turbine in grid generated turbulence. *Sustainable Energy Technologies Assessments*. *11*, 178-185

Moreno, B., Lopez, A. J., & Garcia-lvarez, M. T. (2012). The electricity prices in the European Union. The role of renewable energies and regulatory electric market reforms. *Energy. 48,* 307-313.

Pagnini, L. C., Burlando, M., & Repetto, M. P., (2015). Experimental power curves of small size wind turbines in turbulent urban environment. *Applied Energy 154*, 112-121.

Smith, J., (2010). Effects of Turbulence intensity on the performance of small wind turbines. *Small wind conference,* Stevens Point, WI, USA

Sunderland, K, Woolmington, T, & Blackledge, J., (2015). Small wind turbines in turbulent (urban) environments: A consideration of normal and Weibull distributions for power prediction. *Journal of Wind Engineering and Industrial Aerodynamics, 121*, 70 – 81.

Wagner, H. J. & Mathur, J., (2012). *Introduction to Wind Energy Systems: Basics, Technology and Operation.* Springer Science and Business Media.

Wekesa, D. N., Wang, C., Wei, Y., & Kamau, J. N., (2014). Wind resource assessment and numerical simulation for wind turbine airfoils, in: 2014 *15th International Workshop on Research and Education in Mechatronics (REM),* Egypt, *15*, 1- 9

Wekesa, D. W., Wang, C., Wei, Y., & Louis, D., (2014). Influence of operating conditions on unsteady wind performance of vertical axis wind turbines operating within a fluctuating free-stream: A numerical study. *Journal of Wind Engineering & Industrial Aerodynamics*. *135*, 76-89.

Wekesa, D. W., Wang, C., Wei, Y., & Zhu, W., (2016). Experimental and numerical study of turbulence effect on aerodynamic performance of a small-scale vertical axis wind turbine. *Journal of Wind Engineering and Industrial Aerodynamics* 2016b, *157*, 1-14.

Wekesa, D. W., Wang, C., Wei, Y., Kamau, J.N, & Danao, L.A.M., (2015): A Numerical Analysis of Unsteady Inflow Wind for Site Specific Vertical Axis Wind Turbine: A Case Study for Marsabit and Garissa in Kenya. *Renewable Energy*. *76*, 648-661.

Wekesa, D. Wang, C., Wei, Y., & Louis, D., (2017*).* Analytical and numerical investigation of unsteady wind for enhanced energy capture in a fluctuating free-stream. *Energy 121*,854- 864.

Wekesa, D.W., (2016). *Aerodynamic Loading and Performance of Vertical Axis Wind Turbines under Unsteady Winds*, Unpublished PhD thesis, Ha'erbin Shi, China: Harbin Institute of Technology.

APPENDICES

Appendix I: LabVIEW data logging program display

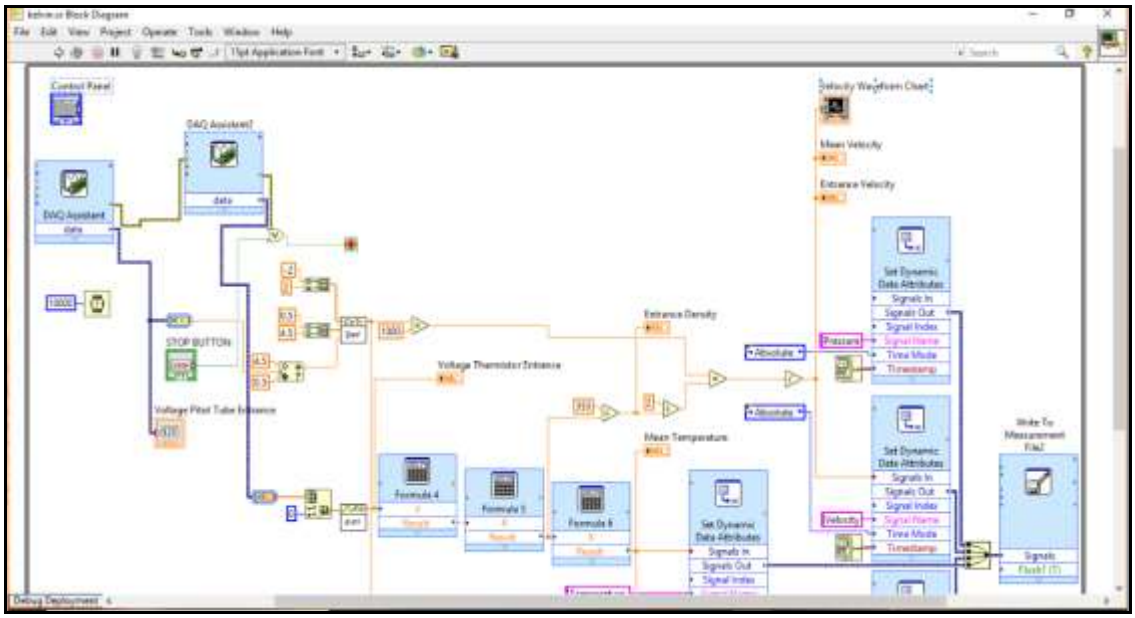

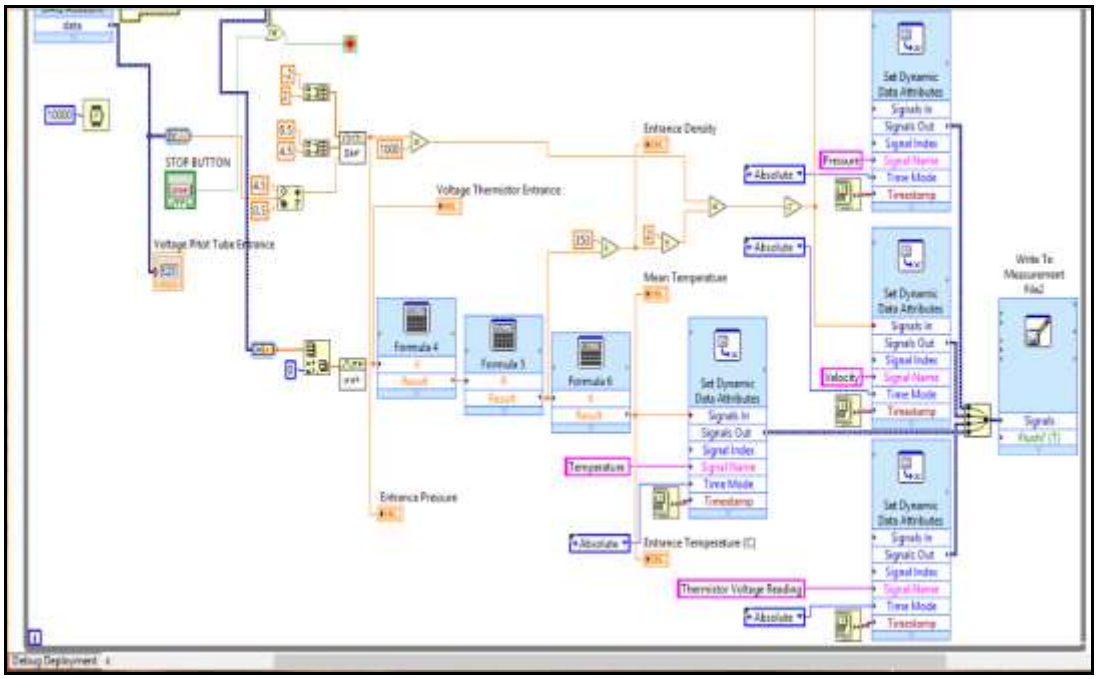

Appendix II: Data display

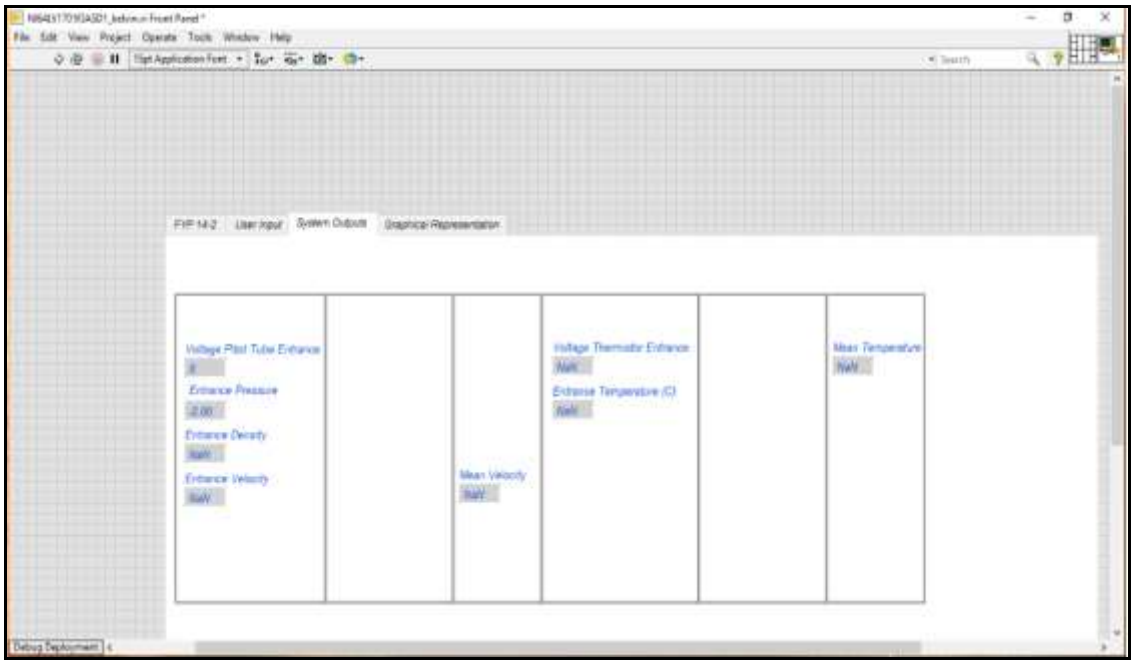

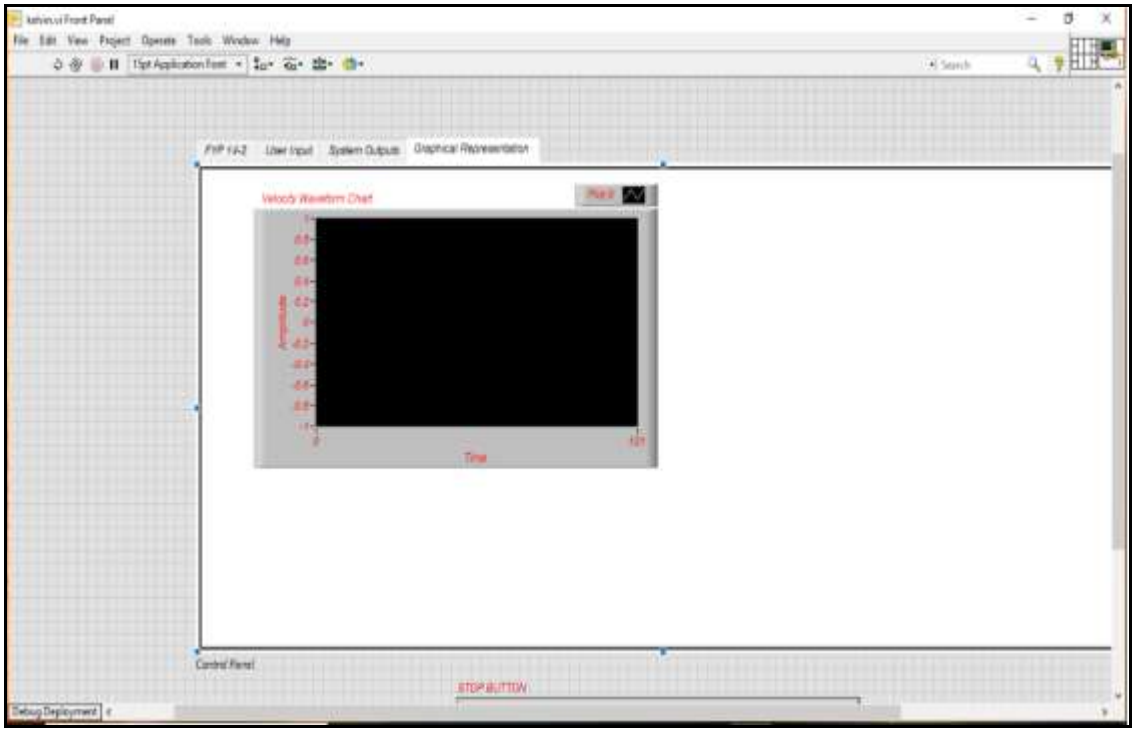
File Edit View Project Operate Tools Window Help
User Input
System Outputs
Graphical Representation
Velocity Waveform Chart
Amplitude
Time
Control Panel
STOP BUTTON
Debug Deployment

Appendix III: Experimental set-up and data collection

Appendix IV: Instrumentation for data collection

Appendix V: Tabulated data for various wind speeds at different times for Uniform and non-uniform conditions

TIME	Uniform	Non-Uniform
10	11.82344	1.985648
20	11.79926	5.8818
30	11.80604	3.2654
40	11.80517	11.75905
50	11.81096	1.231
60	11.83989	2.365987
70	11.8181	1.458799
80	11.79916	9.287056
90	11.8042	13.78938
100	11.8067	10.17451
110	11.81099	3.888878
120	11.81529	13.12716
130	11.80014	4
140	11.84681	1.235488
150	11.81241	4.151224
160	11.81367	4.1559
170	11.84131	1.3254
180	11.81082	7.189826
190	11.81686	8.313899
200	11.8101	2.2213
210	11.82181	1.2321
220	11.81008	2.36546
230	11.83046	7.203341
240	11.83334	3.14258
250	11.81265	2.5874
260	11.83313	11.76204
270	11.82549	10.17757
280	11.82567	8.319097
290	11.82274	15.57218
300	11.82326	7.199679
310	11.81974	2.45687
320	11.84953	5.875882
330	11.81819	11.01969
340		4.15944
350		5.885029

360		1.235487
370		9.301991

Height 15cm VFD 36Hz

Time	**Uniform**	**Non-Uniform**
10	12.53819	7.208794
20	12.53	4.162372
30	12.52	8.32776
40	12.5287	8.332392
50	12.52795	2.888989
60	12.54785	3.114778
70	12.52851	9.303515
80	12.54026	12.50707
90	12.5289	2.222225
100	12.53336	4
110	12.54074	3.889875
120	12.5433	11.76674
130	12.5455	7.210213
140	12.53627	3.2
150	12.54884	2.8888
160	12.53988	1.888878
170	12.53973	3.555588
180	12.53731	7.2046
190	12.54029	4.159947
200	12.54318	10.20369
210	12.54606	8.311499
220	12.54	3.2254
230	12.55246	4.162269
240	12.5538	9.316096
250	12.55384	4.222545
260	12.54	1.23658
270	12.55283	9.31526
280	12.54561	4.166183
290	12.54396	12.47907
300	12.54873	3.7859
310	12.54	2.85694
320	12.5474	3.111121
330	12.54031	5.891178
340	12.538	4.164079
350	12.538	7.21395
360	12.52785	4.12321

370	12.54721	3.698
380	12.54	5.88916
390		11.01291

Height 5 cm VFD 28Hz

Time	**Uniform**	**Non-uniform**
10	8.285416	1.2
20	8.28585	2.475
30	8.286282	3.148
40	8.28965	1.884
50	8.2794	3.648
60	8.2854	4.13573
70	8.283698	4.132
80	8.285399	2.374
90	8.285596	0.884
100	8.285792	5.850137
110	8.285272	2
120	8.285068	3.214
130	8.28	4.13673
140	8.284075	1.238
150	8.28	4.448
160	8.282934	3.464
170	8.284	5.852506
180	8.284707	1.38
190	8.284314	7.168159
200	8.28	5.852171
210	8.283784	2.228
220	8.2819	5.852703
230	8.28457	2
240	8.28695	4
250	8.277178	1.648
260	8.278762	3
270	8.2788	2.846
280	8.278578	3.215
290	8.27999	4.138761
300	8.2793	1.487

310	8.279415	4
320	8.280384	8.276915

Height 5cm VFD 30Hz

Time	**Uniform**	**Non-uniform**
10	9.2544	3.8854
20	9.260541	2.235
30	9.259777	1.3256
40	9.256657	1.888595
50	9.25725	3.456289
60	9.257788	2.98254
70	9.2568	1.88548
80	9.255763	8.272615
90	9.256802	1.215445
100	9.2543	4.135956
110	9.2537	1.888895
120	9.253048	4.13528
130	9.2541	1.889598
140	9.257338	2.88978
150	9.256169	5.850851
160	9.2549	4.137076
170	9.253584	2.48745
180	9.25366	7.167639
190	9.253542	4
200	9.254106	2.223665
210	9.2538	3.568956
220	9.2539	1.325878
230	9.254	4.1232
240	9.254025	1.237
250	9.2536	4.0012
260	9.253315	3.22658
270	9.253531	3.8895
280	9.2534	4.000001
290	9.25255	2.4785
300	9.251703	4.222545
310	9.2526	1.58965
320	9.253456	0.2389
330	9.2529	4.666698
340	9.2542	8.279984

Height 25 cm VFD 30 Hz

Time	**Uniform**	**Non-uniform**
10	9.3227	10.2106
20	9.303588	1.88578
30	9.341808	4
40	9.321758	5.896658
50	9.318942	7.229112
60	9.328066	2.889755
70	9.319768	5.894041
80	9.31183	9.322932
90	9.332725	5.897722
100	9.327949	7.223881
110	9.325014	8.341256
120	9.333276	4.167103
130	9.333045	7.224336
140	9.331646	9.315371
150	9.351057	2.114529
160	9.332503	1.858546
170	9.316838	2.88457
180	9.334613	5.895447
190	9.333596	3.222222
200	9.335612	5.890441
210	9.316611	5.899485
220	9.318381	3.565654
230	9.3299	9.316481
240	9.3265	7.234017
250	9.3245	4.163339
260	9.319164	5.894756
270	9.329782	4.168894
280	9.322412	2.3656
290	9.314074	4.164475
300	9.32365	11.01639
310	9.333224	4.00012
320	9.333614	8.326828
330	9.3274	4.164621
340	9.32035	12.49356
350	9.33	4.175229

360	9.33	5.896923
370	9.335592	10.20003
380	9.324274	13.21212
390	9.323587	16.88787

Height 25 cm VFD 34 Hz

Time	**Uniform**	**Non-uniform**
10	11.02602	5.897587
20	11.01797	5.898092
30	11.01295	11.02732
40	11.00756	8.35056
50	11.02239	13.81335
60	11.02042	11.03808
70	11.03	5.903946
80	11.03616	2.254879
90	11.02623	10.21062
100	11.03655	4.167249
110	11.02071	9.320253
120	11.0225	5.901411
130	11.02429	5.892319
140	11.03564	9.307223
150	11.03455	4.168479
160	11.0157	17.22471
170	11.01757	9.315297
180	11.01472	3.8887
190	11.0341	9.315869
200	11.0382	1.88548
210	11.0132	12.50962
220	11.00647	7.233839
230	11.04032	2.2854
240	11.03021	11.0375
250	11.032	9.326064
260	11.02602	13.81016
270	11.04707	3.222232
280	11.04905	7.226362
290	11.03284	11.7893
300	11.01535	3.66698
310	11.01272	4.17341
320	11.01354	11.7957
330	11.0395	5.892897

Height 35 cm VFD 26Hz

Time	**Uniform**	**Non-uniform**
10	4.1325	1.874597
20	4.13333	8.254768
30	4.132856	2.85469
40	4.132501	9.229325
50	4.133018	4.127037
60	4.134	4.127523
70	4.134751	3.8784
80	4.13335	5.837438
90	4.13322	1.888548
100	4.133231	7.150693
110	4.133143	5.839044
120	4.132687	4.128617
130	4.1328	5.839319
140	4.133434	2.239856
150	4.13364	7.152493
160	4.132496	5.83758
170	4.133611	1.23678
180	4.133924	4.128749
190	4.133701	4
200	4.134222	3
210	4.134388	5.833631
220	4.134552	2.896997
230	4.134972	8.256366
240	4.135899	1.887594
250	4.135112	7.149232
260	4.135	4.126577
270	4.134	4.127387
280	4.133584	2.522369
290	4.1333	4.127208
300	4.132853	4
310	4.132564	3.33223
320	4.133636	5.837704
330	4.132075	4.128224

Height 35 cm VFD 28Hz

Time	**Uniform**	**Non-uniform**
10	5.84604	7.149861
20	5.842497	5.838174
30	5.845698	4.127766
40	5.843266	7.148867
50	5.845948	5.837324
60	5.846075	7.149624
70	5.847888	4
80	5.847356	5.837317
90	5.847425	4
100	5.848468	2.548888
110	5.8467	9.230653
120	5.844628	5.839096
130	5.842364	8.25649
140	5.84726	8.257282
150	5.847353	7.151462
160	5.846212	8.257824
170	5.847001	3.121213
180	5.847618	10.92238
190	5.846785	8.258294
200	5.847202	8.258957
210	5.847995	1.25684
220	5.84254	2.222999
230	5.84237	1.888555
240	5.848231	2.29969
250	5.847909	4.14145
260	5.8483	7.153846
270	5.8425	8.253719
280	5.83995	7.154752
290	5.8425	7.153367
300	5.84569	11.356